CHALMERS
UNIVERSITY OF TECHNOLOGY

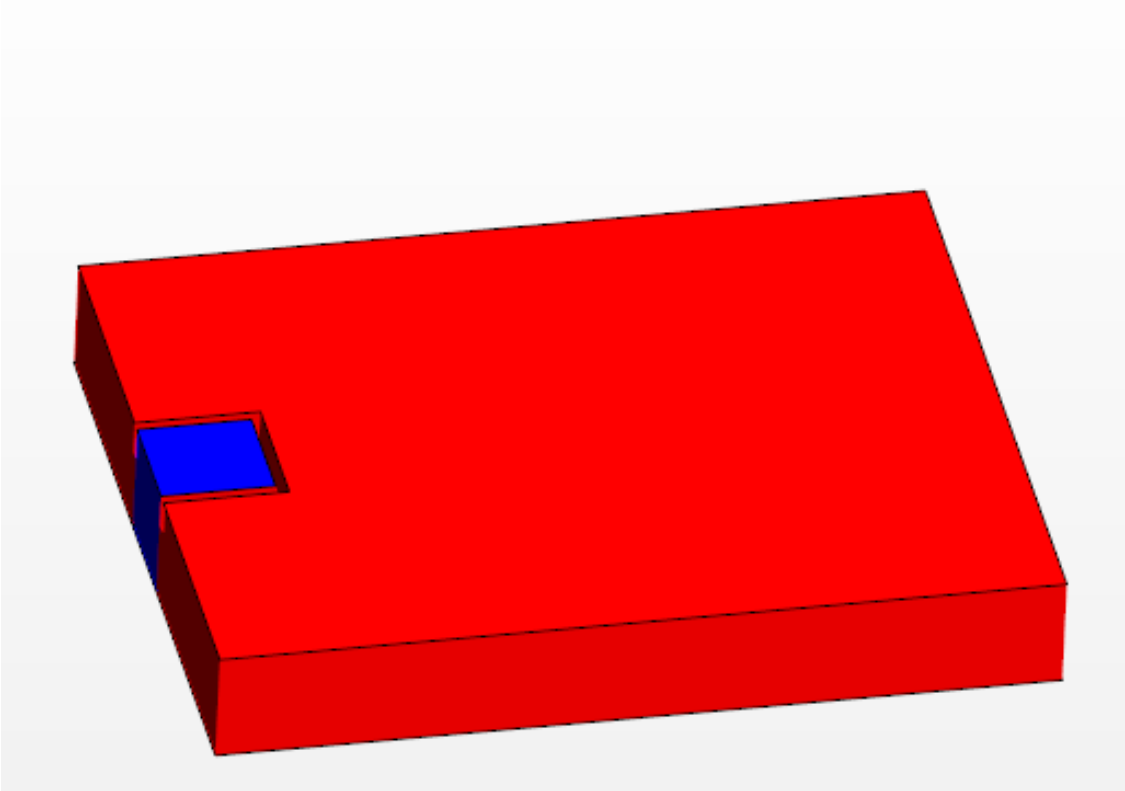

Estimation of the temperature field in an industrial bubbling fluidised bed

Development of a diffusion-type reduced-order model with input from Eulerian-Eulerian multiphase simulation

Master's thesis in Master Programme of Innovative and Sustainable Chemical Engineering

GABRIEL GUSTAFSSON

Department of Mechanics and Maritime Sciences
Chalmers University of Technology
Gothenburg, Sweden 2019

Master's thesis 2019:09

Estimation of the temperature field in an industrial bubbling fluidised bed

Development of a diffusion-type reduced-order model with input from Eulerian-Eulerian multiphase simulation

GABRIEL GUSTAFSSON

CHALMERS
UNIVERSITY OF TECHNOLOGY

Department of Mechanics and Maritime Sciences
Division of Fluid Dynamics
Chalmers University of Technology
Gothenburg, Sweden 2018

Estimation of the temperature field in an industrial bubbling fluidised bed
Development of a diffusion-type reduced-order model with input from
Eulerian-Eulerian multiphase simulation.
GABRIEL GUSTAFSSON

Supervisor: Henrik Ström, Department of Mechanics and Maritime Sciences, Chalmers
Examiner: Srdjan Sasic, Department of Mechanics and Maritime Sciences, Chalmers

Master's Thesis 2019:09
Department of Mechanics and Maritime Sciences
Division of Fluid Dynamics
Chalmers University of Technology
SE-412 96 Gothenburg
Telephone +46 31 772 1000

Cover: Domain division of a sectioned fluidised bed constructed and used in STAR-CCM+

Typeset in LaTeX
Department of Mechanics and Maritime Sciences
Gothenburg, Sweden 2019

Estimation of the temperature field in an industrial bubbling fluidised bed
Development of a diffusion-type reduced-order model with input from
Eulerian-Eulerian multiphase simulation.

Gabriel Gustafsson
Department of Mechanics and Maritime Sciences
Chalmers University of Technology

Abstract

Fluidised bed reactors are widely used in industry today, not at least in the energy sector. A common use case is the combustion and gasification of solid fuels such as coal, but also waste and biomass. Recently, a design proposing a fluidised bed divided into two chambers was presented. The proposed design could be beneficial for processes such as gasification where the residence time of fuel and char should be controlled. This work investigates the feasibility of the proposed design. The main point of investigation is whether the heat transfer between the two chambers will be sufficient as well as whether any gas leakage between the two chambers will occur. As a step in the investigation, a design tool to estimate the average temperature differences in the fluidised bed is developed. In addition, the effective conductivity of such a fluidised bed is investigated by means of Eulerian-Eulerian multiphase simulation. The results indicate that any eventual gas leakage would be minor and that the heat transfer might very well be enough, however further work is needed.

Keywords: fluidisation, heat transfer, fluidised bed reactor, multiphase flow, euler-euler, biomass gasification

Acknowledgements

I want to thank my supervisor, Senior Researcher Henrik Ström, for his encouragement and for many much needed discussions. I would also like to thank Associate Professor David Pallares for his guidance and for always taking the time to answer my many questions. Furthermore, I want to thank my examiner Professor Srdjan Sasic for letting me take my sweet time while finishing this report. Also, my time at the division of fluid dynamics would not have been the same without my colleagues in the "Multiphase group". Coming up at the end I want to thank my father for valuable discussions along the way and of course the rest of my family and friends for their support. Lastly one should note that many of the computations were performed on resources at Chalmers Centre for Computational Science and Engineering (C3SE) provided by the Swedish National Infrastructure for Computing (SNIC).

Gabriel Gustafsson, Göteborg, Mars 2019

Contents

Nomenclature

Greek Symbols

α_{eff}	Effective thermal diffusivity	m^2/s
α	Volume fraction	
$\alpha_{s,max}$	Maximum solids volume fraction	
γ	Granular dissipation rate	$\mathrm{J}/(\mathrm{m}^3 \cdot \mathrm{s})$
κ	Granular diffusion coefficient	$\mathrm{J}/(\mathrm{s} \cdot \mathrm{m}^3)$
λ_s	Solids bulk viscosity	$\mathrm{Pa} \cdot \mathrm{s}$
μ	Shear viscosity	$\mathrm{Pa} \cdot \mathrm{s}$
ϕ	Angle of internal friction	
ρ	Density	kg/m^3
Θ	Granular temperature	$\mathrm{m}^2/\mathrm{s}^2$
τ	Stress-strain tensor	Pa

Roman Symbols

d_p	Particle diameter	m
ΔH_{vap}	Heat of vaporisation	J/kg
$\dot{m}$	Mass flow	kg/s
$\mathbf{P_i}$	Inertial resistance tensor	$\mathrm{Pa} \cdot \mathrm{s}^2/\mathrm{m}^2$
$\mathbf{P_v}$	Viscous resistance tensor	$\mathrm{Pa} \cdot \mathrm{s}/\mathrm{m}$
$\mathbf{q}$	Heat flux	W/m^2

$\mathbf{T}$	Fluid stress tensor	Pa
$\mathbf{I}$	Identity matrix	
$\mathbf{u}$	Velocity	m/s
a	Interfacial area	1/m
C_D	Drag coefficient	
c_p	Specific heat capacity	$\mathrm{J/(kg \cdot K)}$
D_s	Coefficient of particle diffusion	$\mathrm{m^2/s}$
D_{sij}	Strain rate tensor	1/s
e	Restitution coefficient	
E_g	Total energy of the fluid	$\mathrm{W/m^3}$
g_0	Radial distribution function	
H	Total enthalpy	J/kg
h	Heat transfer coefficient	$\mathrm{W/(m^2 \cdot K)}$
H_r	Heat of reaction	kJ/mol
I_{2D}	Second invariant of the deviatoric stress tensor	$\mathrm{1/s^2}$
J_i	Mass flux of species i	$\mathrm{kg/m^2/s}$
k	Heat conduction	$\mathrm{W/(m \cdot K)}$
k_{eff}	Effective thermal conductivity	$\mathrm{W/(m \cdot K)}$
K_{sg}	Interphase momentum exchange coefficient	$\mathrm{kg/(s \cdot m^3)}$
LHV	Lower heating value	J/kg
M	Molar mass	kg/mol

p	Pressure	Pa
q	Heat flux	W/m^2
q_{char}	Heat needed to bring char to bed temperature	J/kg
q_{fuel}	Heat needed to bring fuel to pyrolysis	J/kg
q_{H_2O}	Heat needed to bring moisture to bed temperature	J/kg
Re	Reynolds number	
S_V	Surface to volume ratio	
S_{C1}	Energy source term for char combustion	W/m^3
S_{C2}	Energy source term for drying and devolatilisation	W/m^3
S_{G1}	Energy source term for char gasification	W/m^3
S_{G2}	Energy source term for drying and devolatilisation	W/m^3
S_{net}	Net energy source term	W/m^3
T	Temperature	K
T_{bed}	Temperature of bed	K
V_r	Terminal velocity ratio	
X	Chemical conversion	
Y_i	Mass fraction of species i	

Subscripts

$+$	Positive source term
$-$	Negative source term
col	collisional

daf	Dry ash free fuel
fr	frictional
G	Gasification chamber
kin	kinetic
s	Solid phase
U	Combustion chamber
g	Gas phase

1 Introduction

Fluidised bed reactors (FBRs) have grown to be a well established technology. First applied industrially in chemical process industry for gasification of coal, fluidised bed technology is now applied in many different fields of industry [1]. Applications span various catalytic reactions such as those in fluid catalytic cracking (FCC) [2], non-catalytic reactions like those for roasting ores, and a range of physical operations such as drying, coating, granulation etc [3], [4]. A relatively active field of application is in the energy sector where FBRs are used to good results for combustion of solid fuels, notably waste and biomass [5]. As the industry gets more interested in gasification and pyrolysis of biomass and waste, fluidised bed reactors have increasingly been used for that as well [6].

In a fluidised bed reactor, a bed of particles is made to fluidise, i.e behave more or less like a liquid. The fluidisation is accomplished by injecting gas from below, with a velocity high enough for drag to counteract gravity, suspending the particles [1]. In combustion, this gas is usually air, while in gasification steam is common [4]. Furthermore, as the gas velocity increases, bubbles form in the bed. These bubbles enhance the mixing properties of the bed considerably, especially in the vertical direction, since they carry particles in their wakes. This upward transport of particles and their subsequent descent create a circulating motion within the bed itself [1].

Fluidised bed reactors come with several advantages with regard to processes where solid particles are to be used. A large benefit is that fluidised beds have a more or less uniform temperature distribution. With some exceptions for the larger fluidised beds used for energy conversion, hot spots in the bed are rare even for strongly exothermic reactions [1]. Coupled with good heat transfer between both the gas and available heat transfer surfaces, fluidised bed reactors become an attractive alternative for both exothermic and endothermic reactions at high temperatures. Another benefit is that since the particles can be made small, the available surface area can be rather large. The large area together with the extensive mixing in the bed have the potential to mitigate mass transfer limitations between the gas and the solid [1]. Lastly, the fact that the material is fluidised makes transport and handling of the solid particles easier. Since the particles flow more or less like a fluid they can be transported in pipes and shuttled between different reactors, as is done in FCC [2], or chemical looping combustion [7].

Obviously, there are disadvantages as well. Notable are those of uneven residence times for both gas and particles. Due to the bubbles in the bed, portions of the injected gas will not get as much contact with the solids as the gas that goes in the dispersed part of the bed [1]. Reduced contact time results in lower conversion in turn. The solid particles are also subject to uneven residence times. Due to the extensive mixing it is hard to guarantee

which specific particles get transported to another part of the reactor or another chamber [1]. If further optimisation is to be done, better control over the individual residence times of different particles in the bed would be beneficial [1].

As a way to increase control over the residence time of, lighter, fuel-like particles in a fluidised bed reactor, Zhao *et al.* recently proposed a concept for retrofitting a fluidised bed reactor into a multi-staged reactor with two chambers [8]. A thin wall inserted with an opening at the bottom separates the two chambers. The time that lighter, fuel-like, particles spend in the first chamber is then controlled through varying the pressure inside and thus the bed height. The targeted application as of yet is gasification of biomass together with heat generation. Since the two chambers are separated, except for the small opening at the bottom, the chemical environment in the first chamber can be kept different from that of the second chamber, and by means of additional connections separate collection of any produced gas is made possible [8].

The initial publication on the concept showed promising results. The experimental setup used was a down-scaled cold flow model corresponding to a bed 5 times larger and under hot conditions. It was experimentally demonstrated that fuel-like particles could be made to float on top of the bed in the gasification chamber for as long as needed. Through simulation of the same setup it was also shown that denser particles would tend to sink down into the bed instead [8].

Furthermore, an effort to estimate the effective thermal conductivity of the bed was made. The effective conductivity was said to depend on the bed movement and related to the lateral dispersion coefficient in the bed. For the simulated cold flow setup, the value of the dispersion coefficient was estimated as 0.0018 m^2/s, roughly corresponding to an effective conductivity of 1800 W/mK [8]. Scaling the dispersion value according to the scaling laws used to design the model gives an estimation of the conductivity of the hot upscaled bed around 26000 W/mK [8], [9].

For a future implementation, new questions of a more practical nature arise. The dimensions and placement of the primary chamber need to be decided. And based on the desired operation conditions, such as fluidisation speed, fuel moisture etc the temperature in the bed will vary. Thus, a tool for evaluating different designs and conditions is needed. In addition, investigation into the questions about heat transfer and gas leakage between the chambers is needed in order to evaluate the overall feasibility of the implementation.

This project aims to assess to what degree gas leakage and heat transfer will limit an eventual implementation. In addition, the effect of different designs and operating cases will also be investigated.

To investigate especially the heat transfer, CFD simulation is the most viable route. However, a fluidised bed is a multiphase system, and for the industrial length scales in question, the computation could likely be rather expensive. The multiphase model most likely to handle those scales is an is an Eulerian-Eulerian two phase model [10]. However, as a design tool even the two phase model is too expensive if multiple designs and operating points are to be tried. Thus, this project aims to use the two phase model only as a means to answer the questions about heat transfer and gas leakage. To still aid the design of the chamber, a reduced order model building on knowledge of the gasification process has been developed. Through the combined approach of the two models both the design and feasibility of the implementation has been evaluated.

2 Theory

This study lies at the intersection of many different topics. Gasification, multiphase flow, heat transfer, reaction engineering, and fluidisation are key topics. The following sections are intended to give a brief overview into the most critical concepts.

The first section deals with biomass gasification. Specifically biomass gasification with steam as a gasification agent since that is a proposed route in the upcoming implementation. After that, a short review of the key concepts in the Two Fluid Model (TFM) is presented. Lastly, extra attention is paid to the dominant heat transfer mechanisms in fluidised beds since knowledge of these is the foundation for many of the assumptions made in latter parts of the study.

For in-depth knowledge of the individual topics the reader is advised to consult existing reference works on the subject. For gasification, "Combustion and Gasification in Fluidized Beds" by Basu Prabir can be used as an overview [11]. Regarding heat and mass transfer, the book "Fluidised bed Combustion" by S. Oka comes highly recommended [12]. The Two Fluid model and the closures employed to model systems like fluidised beds are described to a fair degree by the Theory Guide in the open documentation of the MFIX project [13]. However, since the actual models available will differ between various codes, a necessary step is of course to verify by means of the manual for the chosen code.

2.1 Biomass Gasification

Thermal gasification of a solid organic feedstock is a process that has been used for a long time. As noted above, in the petrochemical industry, the gasification of coal has long

been used to supplement natural gas [1]. Recently the process has instead gained interest as a way to mitigate climate change. By gasifying a bio-based feedstock such as wood, the resulting biogas can be treated as a low carbon alternative to natural gas [14], [15].

To simplify, gasification of biomass consists of three main steps: drying, devolatilisation, and char conversion [11], [16]. First any moisture present in the biomass is driven off. The then dry material can be divided into two main fractions, volatiles and char. This dry material then undergoes devolatilisation, here larger molecules in the material are broken down and subsequently driven off as gas. Any compounds formed and driven off in this step are usually referred to as volatiles, even if they are be found in condensed form at ambient temperatures [11] . Finally, the remaining fraction of char, mainly comprised of solid carbon, can be further converted into gas by the addition of a gasification agent, usually steam, carbon dioxide, oxygen or a mixture thereof [16]. Compared to the devolatilisation step, the char conversion is a slower process. This process usually requires longer retention times to reach completion [11], [16].

The system of reactions is extensive and influenced by both the type of feedstock and process parameters [15]. Temperature is one of the main parameters, as well as the choice of gasification agent and the presence of a catalyst [15]–[17]. Various models of different complexity exist for describing the system but the field is far from charted [17]. Since the type of feedstock that can be used is incredibly varied, virtually any biologic material with reasonably low moisture content, it is no surprise that the reaction paths vary as well [15].

Qualitatively, the main components in biogas from thermal gasification are those of hydrogen (H_2), carbon monoxide (CO), carbon dioxide (CO_2), water (H_2O) and methane (CH_4). A certain fraction of longer hydrocarbons (C_xH_y) are usually present as well but seldom above a few percent [11], [17]. The composition here refers to cold gas after it has been collected and any longer hydrocarbons have been condensed out and separated as tar. The hot, so called "raw gas", has a significantly more complex make-up and can also be heavily diluted, depending on the gasification agent [16].

As noted before, in the proposed implementation, steam is the intended gasification agent. In gasification with steam, an idealised model reaction concerning the char gasification is that of pure carbon with water [18] :

$$C(s) + H_2O \longrightarrow H_2 + CO \qquad \Delta H_r = 131.3\ kJ/mol \tag{1}$$

This pathway leads to a biogas containing a larger fraction of hydrogen and carbon monoxide compared to the inert carbon dioxide present. This higher ratio of burnable species in

turn leads to a higher heating value. A process using steam will of course be more energy intensive, and require a good heat recovery system. However, steam tends to produce the gas with the highest heating value [19].

The temperature at which the gasification is conducted heavily influences gas yield and heating value of the produced gas. In general, the higher the temperature the more extensive char gasification and thus higher gas yield [16]. For gasification conducted in a fluidised bed, a commonly used temperature is 850 $°C$. At temperatures above 900 $°C$, there is a risk that sintering of the sand in the bed will occur [12], [20]. Some degree of gasification happens at lower temperatures as well. The initial devolatilisation step will occur even at temperatures around 300-400 $°C$ [21]. But at these temperatures, char gasification is virtually nonexistent and there will be a large amount of longer hydrocarbons present in the raw gas, which when cooled will condense out as tar [16], [21].

Of the three steps described, the drying step is the most energy demanding; even more so if the biomass used has a high moisture content. After that, the char gasification is potentially the second most demanding, depending on what degree of char conversion that is desired. The devolatilisation step however, can be one to three magnitudes lower in comparison [22]. Some authors even report the devolatilisation as an exothermic process [23].

2.2 Two fluid Model

As mentioned in the introduction, for the more detailed modelling the study makes use of an Eulerian-Eulerian (E-E) framework. This framework means that both the solid and the fluid phase is treated with a continuum description [10], [24]. A common name for this treatment in the field of fluidisation is the "Two Fluid Model" (TFM) since, at the top level, the particle phase is described using equations resembling those used for a fluid. The main reason for using an E-E framework is not that it is more accurate, or easy to implement, but that of size. A particulate system of industrial size simply contains too many entities to fully resolve them. A continuum description is therefore a necessary averaging process in order to reduce the data that has to be handled [10].

The governing equations in the two fluid model, seen in Table 1, look more or less like the Navier-Stokes equations. The obvious difference being that they are weighted with the respective volume fraction for each phase as well as the inclusion of a coupling mechanism [24]. The real difference, however, lies in the models employed to close the equations. For the continuous phase, the treatment is usually the same as for a single phase flow. Notable for the fluid is that the stresses are expressed by means of the viscosity for the

material studied. Viscosity, however, is a molecular concept. For a "fluid phase", not made up of molecules but of particles, the concept of viscosity cannot be defined in the same fashion. The stresses then need to be handled through some other model instead. The conventional model of choice, that is used to some success, is the Kinetic Theory of Granular Flow [25].

2.2.1 Kinetic Theory of Granular Flow

In the framework of the kinetic theory of granular flow (KTGF), the particles that make up the continuum are treated somewhat analogous to that of molecules in a dense gas [25]. The continuum could thus be thought of like a form of particulate gas. Kinetic gas theory proposes that in a volume of gas there are two mechanisms for momentum transfer, translation and collision [26]. Translation, being that of gas molecules moving from one point to another. Collision, that of gas molecules colliding in elastic collisions and thus sharing momentum through the collision. Similarly, the kinetic theory of granular flow only considers momentum transfer by the same two mechanisms. To say that, for particulate flows, these mechanisms are sufficient in all situations is an idealisation [27]. However, there are definitely systems in which these two mechanisms could at least be the dominant forms of momentum transfer [25], [27].

Furthermore, kinetic gas theory is based on probability, much else would be unreasonable due to the enormous amount of entities that would have to be handled otherwise. In this sense, at a certain point in space, there is a certain possibility of finding a molecule with a specific velocity. This probability is what determines both the chance of a collision happening as well as what amount of momentum would be transferred in such a collision [26].

Still in analogy, the same probabilistic reasoning can be ascribed to the particles in a granular continuum, albeit with some modification. The modification is needed since molecules and particles differ somewhat in how they interact. Firstly, molecules are thought to collide in elastic collisions, while particles generally lose at least some of their energy to heat. Thus, a flow of particles is by nature more dissipative than that of a gas [25]. This dissipation needs to be modelled. Another difference is that, in gas theory, molecules are thought to translate through a volume independently of each other, the so called molecular chaos assumption. Particles, however, can interact somewhat by means of the interstitial fluid, and as such can not be assumed to move independently in all cases. Accordingly, the probability of two particles meeting and colliding has to be adjusted [25].

To go from the scale of a probability distribution to that of a continuum, once more an

averaging procedure is needed. The familiar transport equation form of the governing equations in table 1 is obtained by first introducing a transport equation for the probability function itself [25]. Then, multiplying that equation with the relevant quantity to be described, and employing an averaging procedure, averaging over all possible velocity configurations. After repeating this process for the three quantities of mass, momentum and kinetic energy the corresponding transport equations emerge after significant rearrangement [25].

Perhaps the most notable quantity emerging from the resulting system of equations is that of granular temperature. Similar to molecular temperature, quantifying the fluctuating isotropic motion of molecules in a substance, granular temperature quantifies the fluctuating motion of particles in the continuum [10]. It can be thought of like a measure of how much kinetic energy that is tied up in fluctuating motion. The transport equation for this is shown in equation 2:

$$\frac{\partial(\alpha_s \rho_s \Theta_s)}{\partial t} + \boldsymbol{\nabla} \cdot (\alpha_s \rho_s \Theta_s \mathbf{u_s}) = (-p_s \mathbf{I} + \tau_\mathbf{s}) : \boldsymbol{\nabla}(\mathbf{u_s}) + \kappa \boldsymbol{\nabla} \Theta_s - \gamma - 3K_{sg}\Theta_s \qquad (2)$$

Here, the two terms to the left of the equal sign signify accumulation and advection of granular energy, respectively. To the right of the equal sign, the first term represents production of granular temperature due to shear in the particle phase. The second term represents diffusive transport of granular temperature with κ as the granular diffusion coefficient. The third term γ is the dissipation of granular energy and finally the last term represents dissipation due to interaction with the fluid phase [10].

In this work, the granular temperature transport equation has been simplified by assuming that the production and dissipation of granular energy is in equilibrium. Neglecting the terms for advection and diffusion, ie $\boldsymbol{\nabla} \cdot (\alpha_s \rho_s \Theta_s \mathbf{u_s})$ and $\kappa \boldsymbol{\nabla} \Theta_s$, the equation can be turned into an algebraic equation instead. This is a known treatment but not always valid. The decision to use the algebraic version in this work was motivated by other studies reporting that for bubbling fluidised beds, the choice of full or algebraic granular temperature transport had little impact [10], [13]. Since the algebraic version also comes with a lower computational cost, up towards 20 % according to Wachem *et al.* [10], this was seen as sufficient motivation to use it over the full version. The used algebraic equation together with the necessary sub-models is presented in Table 1.

By means of the granular temperature and further sub-models, the stresses and solid pressure terms can be closed. The last remaining term to close is the inter-phase momentum transfer. This is handled by means of a drag law. However, an assembly of particles interact differently with a fluid phase depending on how tightly packed the particles are.

Thus, the drag law used has to be able to handle changing conditions. The drag law used in this work, developed by M. Syamlal and T.J O'Brien, handles changing conditions by relating the drag force to the terminal velocity of the solid phase and then expressing that terminal velocity through an existing correlation by Garside and Al-Dibouni [13], [28]. The correlation then provides the sought relation with volume fraction and particle Reynolds number. The drag law and terminal velocity correlation are both shown in table 1.

Table 1: The equations making up the framework of the TFM-model used.

Gas phase continuity	$\frac{\partial(\alpha_g \rho_g)}{\partial t} + \boldsymbol{\nabla} \cdot (\alpha_g \rho_g \mathbf{u_g}) = 0$
Solid phase continuity	$\frac{\partial(\alpha_s \rho_s)}{\partial t} + \boldsymbol{\nabla} \cdot (\alpha_s \rho_s \mathbf{u_s}) = 0$
Gas phase momentum balance	$\frac{\partial \alpha_g \rho_g \mathbf{u_g}}{\partial t} + \boldsymbol{\nabla} \cdot (\alpha_g \rho_g \mathbf{u_g} \mathbf{u_g}) = -\alpha_g \boldsymbol{\nabla} p + \boldsymbol{\nabla} \cdot \tau_\mathbf{g} + \alpha_g \rho_g \mathbf{g} + K_{sg}(\mathbf{u_s} - \mathbf{u_g})$
Solid phase momentum balance	$\frac{\partial \alpha_s \rho_s \mathbf{u_s}}{\partial t} + \boldsymbol{\nabla} \cdot (\alpha_s \rho_s \mathbf{u_s} \mathbf{u_s}) = -\alpha_s \boldsymbol{\nabla} p - \boldsymbol{\nabla} p_s + \boldsymbol{\nabla} \cdot \tau_\mathbf{s} + \alpha_s \rho_s \mathbf{g} + K_{sg}(\mathbf{u_g} - \mathbf{u_s})$
Gas phase energy balance	$\frac{\partial \alpha_g \rho_g H_g}{\partial t} + \boldsymbol{\nabla} \cdot (\alpha_g \rho_g H_g \mathbf{u_g}) = -\boldsymbol{\nabla} \mathbf{q_g} - \alpha_g \boldsymbol{\nabla}(p) + \boldsymbol{\nabla} \cdot (\tau_\mathbf{g} \cdot \mathbf{u_g}) + S_{g,net}$
Solid phase energy balance	$\frac{\partial \alpha_s \rho_s H_s}{\partial t} + \boldsymbol{\nabla} \cdot (\alpha_s \rho_s H_s \mathbf{u_s}) = -\boldsymbol{\nabla} \mathbf{q_s} - \alpha_s \boldsymbol{\nabla}(p) + \boldsymbol{\nabla} \cdot (\tau_\mathbf{s} \cdot \mathbf{u_s}) + S_{s,net}$
Gas phase species balances	$\frac{\partial \alpha_g \rho_g Y_{g,i}}{\partial t} + \boldsymbol{\nabla} \cdot (\alpha_g \rho_g Y_{g,i} \mathbf{u_g}) = -\boldsymbol{\nabla} \alpha_g \mathbf{J_g}, \mathbf{i} + S_{g,i}$
Interphase exchange coefficient [13]	$K_{sg} = \frac{3}{4} \frac{\alpha_s \alpha_g \rho_g}{V_r^2 d_p} C_D \lvert \mathbf{u_s} - \mathbf{u_g} \rvert$, with [29]: $C_D = \left(0.63 + \frac{4.8}{\sqrt{\frac{V_r}{Re_s}}}\right)^2$ and [28]:
	$V_r = \frac{1}{2}\left[A - 0.06 Re_s + \sqrt{(0.06 Re_s)^2 + 0.12 Re_s (2B - A) + A^2}\right]$
	$A = \alpha_g^{4.14}, \qquad B = \begin{cases} 0.8 \alpha_g^{1.28}, & \alpha_s \geq 0.15 \\ \alpha_g^{2.65}, & \alpha_s < 0.15 \end{cases}, \qquad Re_s = \frac{d_p \rho_g \lvert \mathbf{u_s} - \mathbf{u_g} \rvert}{\mu_g}$
Solids pressure [25]	$p_s = \alpha_s \rho_s \Theta_s + 2\rho_s (1+e) \alpha_s^2 g_0 \Theta_s$

Granular Temperature (algebraic) [13]

$$\Theta_s = \left\{ \frac{-K_{1s}\alpha_s D_{sii} + \sqrt{K_{1s}^2\alpha_s^2 D_{sii}^2 + 4K_{4s}\alpha_s[K_{2s}D_{sii}^2 + 2K_{3s}(D_{sij}D_{sij})]}}{2\alpha_s K_{4s}} \right\}^2$$

$$K_{1s} = 2(1+e)\rho_s g_0, \qquad K_{2s} = \frac{4d_p\rho_s(1+e)\alpha_s g_0}{3\sqrt{\pi}} - \frac{2}{3}K_{3s}$$

$$K_{3s} = \frac{d_p\rho_s}{2}\left\{ \frac{\sqrt{\pi}}{3(3-e)}[0.5(3e+1) + 0.4(1+e)(3e-1)\alpha_s g_0] + \frac{8\alpha_s g_0(1+e)}{5\sqrt{\pi}} \right\}$$

$$K_{4s} = \frac{12\big(1+e^2\big)\rho_s g_0}{d_p\sqrt{\pi}}$$

Radial distribution function [25] [30]

$$g_0 = \frac{3}{5}\left[1 - \left(\frac{\alpha_s}{\alpha_{s,max}}\right)^{1/3}\right]^{-1}$$

Solid phase shear stresses

$$\tau_{\mathbf{s}} = \alpha_s\mu_s\big(\boldsymbol{\nabla}\mathbf{u_s} + \boldsymbol{\nabla}\mathbf{u_s}^T\big) + \alpha_s\left(\lambda_s - \frac{2}{3}\mu_s\right)\boldsymbol{\nabla}\cdot\mathbf{u_s}\mathbf{I}$$

Solid phase shear viscosity

$$\mu_s = \mu_{s,col} + \mu_{s,kin} + \mu_{s,fr}$$

Solid phase collisional viscosity [13] [31]

$$\mu_{s,col} = \frac{4}{5}\alpha_s\rho_s d_p g_0(1+e)\left(\frac{\Theta_s}{\pi}\right)^{1/2}$$

Solid phase kinetic viscosity [13]

$$\mu_{s,kin} = \frac{\alpha_s\rho_S d_p\sqrt{\Theta_s\pi}}{6(3-e)}\left[1 + \frac{2}{5}(1+e)(3e-1)\alpha_s g_0\right]$$

Solid phase frictional viscosity [32]

$$\mu_{s,fr} = \frac{p_s sin\phi}{2\sqrt{I_{2D}}}$$

Solid phase bulk viscosity [25]

$$\lambda_s = \frac{4}{3}\alpha_s\rho_s d_p g_0(1+e)\left(\frac{\Theta_s}{\pi}\right)^{1/2}$$

2.2.2 Mesh concerns in the Two Fluid Model

Multiphase simulations of this type quickly become quite resource-intensive, as well as time-consuming due to the small timesteps required. To be able to simulate enough timesteps within timeframe of the project, it is desirable to speed up each inner iteration by using a mesh no finer than necessary.

A fast simulation is not worth much if the results it provides are unphysical though. The general rule of thumb is that a cell side as small as 10x the particle diameter is what is required to properly resolve any clustering effects in the system [33], [34]. However, since the domain is of an industrial size, such a fine mesh would result in a number of cells in the order of 10^8 which is too much given the computational resources available.

Fortunately as it were, some authors argue that, for certain fluidised bed systems and larger particle sizes clustering effects become less significant, and coarser meshes can be used [33], [35]. In an article by Cloete *et al.* it is argued that for particle sizes close to 1 mm a grid size as large as 100 particle diameters can be used. This would make a simulation of the entire bed feasible. However, this value is somewhat of an outlier, and not validated by experimental data. Uddin and Coronella suggest values closer to 20 or 30 particle diameters. Another approach currently under development is to use subgrid models based on finely resolved TFM simulations to account for the unresolved scales of coarser simulations [34], [35]. While this approach has shown some promising results, these kind of models are still on a research stage and not in industrial or commercial use.

To conclude, without using a rather fine grid of around 10 - 20 particle diameters, no generally accepted solution exists. The resulting error will likely vary greatly from case to case and code to code. In order to estimate the error, some kind of verification study is thus needed on a per case basis.

2.3 Heat transfer in bubbling fluidised beds

As already noted, fluidised beds are favoured in part due to their relatively uniform temperature profile. The fluid-solid energy transfer is heavily enhanced by the high interfacial area provided with the bed and due to the shear thermal mass of the sand, any temperature fluctuations tend to be rather minor [1], [12]. However, in a setup such as this where part of the bed will be subject to an entirely different heat load, heat transfer, especially in the lateral direction could potentially be critical.

Out of the possible mechanisms for heat transfer in the bed, the most significant one by

far is thought to be transfer through the motion of the particles [12]. I.e the movement of hot particles to colder regions of the bed. Compared to the heat moved by the fluid, once again due to the thermal mass of the sand, the convective heat transfer by the solid is magnitudes higher [1], [12].

In the book "Fluidised bed combustion", Oka and Anthony present the following relationship for the heat flux in a fluidised bed [12].

$$q = -D_s \rho_p c_p \alpha_s \frac{\mathrm{d}T}{\mathrm{d}x} = -k_{eff} \frac{\mathrm{d}T}{\mathrm{d}x} \tag{3}$$

Here D_s is the coefficient of particle diffusion, or more correctly referred to as particle dispersion coefficient. Rearranging equation 3, it can be seen that the effective thermal diffusion is taken as equal to that of the particle diffusion.

$$a_{eff} = \frac{k_{eff}}{\rho_p c_p \alpha_s} = D_s \tag{4}$$

By noting this relationship, it becomes possible to make predictions of the thermal diffusivity based on the effective solid particle mixing using experimental data or correlations. In the previous study by Zhao *et al.* equation 3 was used to this end.

Regarding particle mixing, it is well established that the major cause of mixing is that of bubble motion [12], [36]. The mixing is also known to be an order of magnitude greater in the axial direction than in the radial direction. This is due to particles being transported through drag in the wakes of bubbles [12]. Furthermore, the degree of mixing is heavily influenced by the geometry of the setup studied [12], [37] . Generally, it is not possible to extrapolate experimental data on particle mixing from smaller experimental setups to beds of industrial sizes since the bubbles scale with the available volume. Thus, to get conclusive results, experimental data in full- or pilot-scale are needed which as of yet are scarce.

Hydrodynamically downscaled experiments performed by Sette *et al.*, report particle dispersion values for a corresponding upscaled bed with the dimensions of 1.5 x 1.5 m on the order of 10^{-2} m^2/s [38]. This dispersion value would correspond to an effective conductivity on the order of 10^4 W/mK. Similarly, the simulations performed on the downscaled model in the previous study on the investigated reactor concept by Zhao *et al.* resulted in an upscaled value of around $3.6 \cdot 10^4$ W/mK. Experiments not on bed solids mixing but on fuel mixing report particle dispersion values even approaching an order of magnitude of

10^{-1} m^2/s [36], corresponding to a conductivity of 10^5 W/mK even. None of the reported results are on beds of the same size or larger than the one intended for the future retrofit however. Furthermore, it is reasonable to assume that some difference exists between fuel particles and bed materials in terms of mixing [36].

Shifting focus to the solid-fluid heat transfer. The high interfacial area of the bed provides a rather efficient heat transfer between phases. According to S., Oka, air entering the fluidised bed generally needs to travel less than 15 cm to reach bed temperature [12]. This happens even though the corresponding heat transfer coefficient systems like these is rather low, 6-25 W/m^2K [12]. For a system of spherical particles of diameter d_p, the ratio between surface area and volume, S_V, can be expressed like

$$S_V = \frac{6\alpha_s}{d_p} \tag{5}$$

For a general particulate system the maximum volume fraction observed is around 63 %. For spheres with a diameter of 1 mm equation 5 yields a maximum area of ≈ 3800 m^2/m^3, for smaller particles the area obviously increases further. Thus, even in a small volume the product of heat transfer coefficient and area will still be rather high.

3 Method

A logical first step was to identify important parameters and physical processes relevant to an the industrial bubbling bed that was targeted for a retrofit. Some inquiries about various operating parameters as well as the design of the bed were made and some preliminary information obtained. This starting information is presented in Table 2.

Table 2: Summary of the starting information provided.

Width [m]	5.9	Heat load [MW]	85
Length [m]	7.4	Gas demand [MW]	15
Static bed height [m]	0.55	Air temp [°C]	200
Particle diameter [mm]	0.95	Steam temp [°C]	200

As visible from Table 2, the dimensions of the existing bed as well as the loads on each chamber were known. Not decided, however, was the placement and dimensions of an eventual gasification chamber. Furthermore, these parameters were assumed to depend

on multiple factors such as hydrodynamics, intra-bed heat transfer, fuel mixing and the existing construction.

To understand what limitations existed due to construction related concerns, a meeting was held with the company eventually responsible for conducting the retrofit. The most notable outcome of this meeting was that the most suitable position for the gasification chamber was deemed to be in one of the corners or along one side of the bed. At this meeting a somewhat arbitrary set of dimensions for the gasification chamber was chosen as to have something to work with. The intention was to verify and update these dimensions as information regarding the limiting factors becomes more clear. The decided arrangement can be seen in Figure 1.

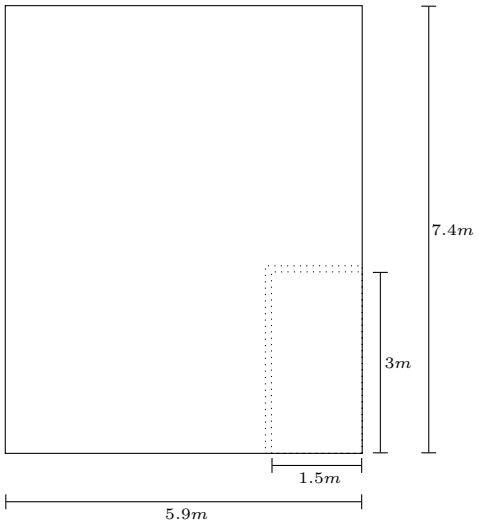

Figure 1: The starting layout of the gasification chamber in the bed. The thickness of the dividing wall is as of yet variable between 0.05 and 0.2 m

At the time, heat transfer was assumed to be one of the more prominent restricting factors affecting the design. However, just how restricting was yet to be seen. To get a preliminary estimation, it was decided to make a simplified model to investigate how the temperature field would change given different design choices.

In addition to the questions about geometry, another initial question was how a fine grid that would be required to properly describe the system. Only a few of the studies on mesh independence actually treat systems of this size. Thus, to find out what size that would be needed for the studied system it was decided to also conduct a shorter mesh study on a smaller domain before moving on to the detailed simulation.

3.1 Simplified heat transfer model

As noted, the simplified model was constructed in order to provide preliminary data on how critical the effects of heat transfer would be on the design. In addition, a sufficiently cheap model, in terms of computational power required, was sought as to allow multiple different designs to be tested. To get a sufficiently cheap model, the velocity field of the bed material was not resolved. Thus, in the simplified model the bed is treated as a stationary material with uniform porosity. Through this material air flows with a set inlet temperature. To further minimise the resources needed, the model is stationary in time as well.

The lateral heat transfer through the domain is governed by an effective conductivity in the bed material. The vertical heat conduction in the bed is then taken as 10 x the lateral heat conduction, reflecting that the vertical mixing in fluidised beds tends to be around one order of magnitude larger than the lateral mixing [12]. By coupling the energy balance of the bed material with that of the fluidising media, convective heat transfer is taken into account as well. Furthermore, the density of the fluidising media is described by the ideal gas law to capture the velocity increase as the fluid is heated to bed temperature.

The governing equations in this model is two energy balances, one for each phase, as well as momentum and continuity equations for the fluid phase. The equations are summarised in Table 3. Since the bed material is stationary and uniform the volume fractions in Table 3 are constant and uniform throughout the domain.

The driving force for the heat transfer is given by source and sink terms applied on the solid energy balance as shown in Figure 2. The sink and source terms are represented in the governing equations by the term S_{net}.

The system is initialised with a uniform temperature of 850 $°C$ and a vertical flow of air corresponding to the inlet velocity adjusted to match the volume fraction of air in the domain. Regarding the boundary conditions for the model, they can be found summarised in Table 4.

The source terms as well as the inlet velocities were calculated from a given load on each chamber. This calculation is described further in section 3.2. Notably, however, different fuel moisture content and degrees of char gasification result in different inlet velocities. As such the values presented in Table 4 are just examples of typical values.

The constant volume fractions in the model are set by means of an assumed porosity. The porosity was chosen based on initial simulations of the unaltered bed. These simulations

Table 3: Governing equations for the simplified model

Fluid phase continuity	$\frac{\partial \alpha_g \rho_g}{\partial t} + \boldsymbol{\nabla} \cdot (\alpha_g \rho_g \mathbf{u}) = 0$
Fluid phase momentum balance	$\frac{\partial \alpha_g \rho_g \mathbf{u}}{\partial t} + \boldsymbol{\nabla} \cdot (\alpha_g \rho_g \mathbf{u}\mathbf{u}) = -\alpha_g \boldsymbol{\nabla} p + \boldsymbol{\nabla} \cdot (\alpha_g \mathbf{T}) - \alpha_g \mathbf{P_v} \mathbf{u} - \alpha_g \mathbf{P_i} \lvert\mathbf{u}\rvert \mathbf{u}$
Fluid phase energy balance	$\frac{\partial \alpha_g \rho_g E_g}{\partial t} + \boldsymbol{\nabla} \cdot (\alpha_g \rho_g H_g \mathbf{u}) = -\boldsymbol{\nabla}(\alpha_g \mathbf{q_g}) + \boldsymbol{\nabla} \cdot (\alpha_g \mathbf{T} \cdot \mathbf{u}) + ah(T_s - T_g)$
Solid phase energy balance	$\frac{\partial \alpha_s \rho_s E_s}{\partial t} = -\boldsymbol{\nabla}(\alpha_s \mathbf{q_s}) + ah(T_g - T_s) + S_{net}$
Definitions:	
Solid conductive heat flux	$\mathbf{q_s} = \mathbf{k_s} \boldsymbol{\nabla} T$
Solid heat conductivity	$\mathbf{k_s} = \frac{\mathbf{k_{eff}} - k_g \alpha_g}{\alpha_s}$

showed an average volume fraction of particles in the fluidised state around 0.43.

The value used for the effective conductivity was given by the downscaled value calculated in the previous study by Zhao *et al.*, adjusted with a scaling factor. The scaling factor was added to account for the much bigger domain compared to the experimental equipment used by Zhao *et al.* Two different cases were tried, scaled by a factor 20 and 100, respectively. A scaling of 20 results in a value of 36000 W/mK, closer to the upscaled value from Zhao *et al.* However, the bed considered for future implementation is larger than the corresponding upscaled bed from the previous study. In addition, studies on dispersion of fuel particles in fluidised beds approaching industrial sizes suggest a value on the order of 10^5 [36][37], thus a scaling of 100 was tried as well. In the later parts of the project, intermediate values of the scaling factor were also tried.

For the coupling between the phases, the heat transfer coefficient, h, had a value of 10 $\frac{W}{m^2\,K}$. This value corresponds to a representative heat transfer coefficient for a gas-solid system as mentioned before [12]. The interfacial area was taken as 1000 $\frac{m^2}{m^3}$. This decision was based on the observation that the value for spherical sand particles would be about 2400 $\frac{m^2}{m^3}$ with the assumed porosity; due to stacking and clustering, this would be reduced significantly. In hindsight this value might have been overly conservative. Regardless of which, without any further information, the value is to be regarded as no more than an

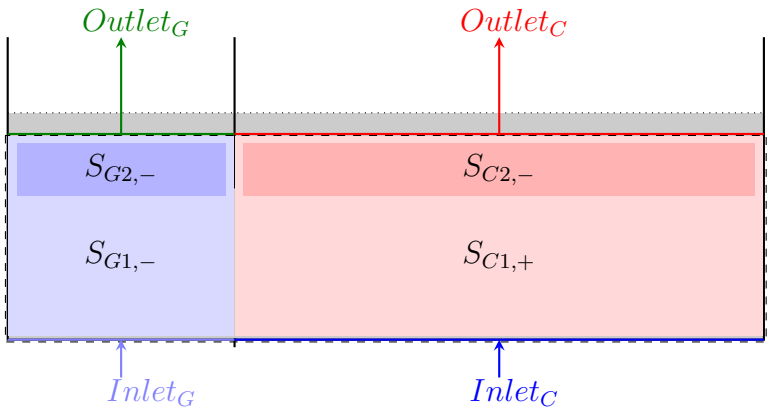

Figure 2: The arrangement of source terms for the simplified model. The negative subscripts indicate sink terms and the positive a source term. The system boundary is indicated by the dashed line.

Table 4: Specification of boundary conditions for the simplified model.

Boundary	Flow specification	Temperature specification
$Inlet_G$	Velocity inlet : $u = 0.41\ m/s$	$T = 200\ °C$
$Inlet_C$	Velocity inlet : $u = 0.84\ m/s$	$T = 200\ °C$
$Outlet_C$	Pressure outlet : $p = 1\ atm$	$T = T_{bed}$
$Outlet_G$	Pressure outlet : $p = 1\ atm$	$T = T_{bed}$
Walls	No-slip condition	Adiabatic

order of magnitude estimate.

The flow of air through the domain was included solely to provide vertical heat transfer. As such its movement was restricted to the vertical axis. While this treatment is an obvious simplification, it should be noted that no realistic flow pattern would be obtainable without also solving for the movement of the bed material. For the vertical pressure drop over the bed the Ergun equation was used. While there may be correlations better suited to fluidised beds, the Ergun equation was easily implemented and deemed sufficient for this first estimation.

The division of the source terms over four different locations was based on the experimental observations in the previous study by Zhao *et al.* The top terms, S_{G2} and S_{C2} represent

the energy needed to heat and dry the floating biomass. The remaining terms are spread evenly over their respective domains, reflecting that the char particles would sink and follow the bed movement. S_{C1} represents energy gained from char combustion and S_{G1} energy needed for char conversion into gas.

3.2 Calculation of source terms

The starting point for estimation of the source terms was the loads and temperatures presented in Table 2. In addition to these values it was said that the mean temperature of the bed should be 850 $°C$, corresponding to the operating temperature of the unaltered bed. The gasification chamber would be fluidised with steam to increase the fuel value of the cold gas. The fuel used in the retrofitted FBR would be the same as before the retrofit, i.e forestry litter, bark and wood chips from pine and fir.

Aside from these starting restrictions imposed by the current case, several important factors worthy of investigation had been identified at the early stages of the project. Out of these factors, the degree of char conversion required as well as the moisture content of the gasification feedstock was deemed the most critical to the process. As such these parameters are made variable in the calculation. Other factors that were identified include the elemental composition of the fuel, the desired gas composition as well as the char yield of the fuel. These latter factors have not been thoroughly investigated yet.

The processes most responsible for removing heat from the domain were considered to be heating, drying, and devolatilisation of the fuel and gasification feedstock as well as the reaction enthalpy needed to sustain the char gasification reaction. The process responsible for adding heat to the domain is of course the combustion of biomass. However, only the combustion of char is taken into account. This decision is due to the assumption that most volatiles would be carried upward and combust in a region above the bed. Since that region is outside the system boundary, and convection would carry the heat further upward, that heat is not included. However, one could argue that some of that heat indeed does reach the bed, through radiation. That radiative contribution was not investigated however.

The calculation of source terms was done in Python code and most thermodynamical data, at least for pure gaseous compounds was obtained through use of the nasa9 polynomials accessed through the package `thermopy`. In essence, the calculation for the gasification chamber consisted of calculating the composition of the product gas, and from that get a heating value and a resulting massflow of biomass. The massflow of biomass would in turn correspond to a certain heating demand. Several assumptions and simplifications

were done on the way, most of them should be made clear in the following description.

3.2.1 Gasification chamber

To develop a model to go from fuel composition to cold gas composition is a task that was deemed out of scope for the current study. Instead, a well documented case from the Chalmers dual fluidised bed gasifier was used as a reference. The parameters used from this case are shown in Table 5

Table 5: The key parameters used from the reference case. The acronym daf stands for "dry ash free fuel". Note also that some gas species are omitted in comparison to those presented by Larsson et al. *[16].*

Yield char	$[\frac{kg}{kg\ daf}]$	5.9	n_{CO}	$[\frac{mol}{kg\ daf}]$	12.1
Steam-Biomass ratio	$[\frac{kg\ steam}{kg\ daf}]$	0.7	n_{H_2}	$[\frac{mol}{kg\ daf}]$	7.5
Air-Fuel ratio	$[\frac{kg\ air}{kg\ daf}]$	7.22	n_{CO_2}	$[\frac{mol}{kg\ daf}]$	4.05
Fuel heating value	$[\frac{MJ}{kg\ daf}]$	19.03	n_{CH_4}	$[\frac{mol}{kg\ daf}]$	4.01
Total gas yield	$[\frac{mol}{kg\ daf}]$	29.35	$n_{C_2H_4}$	$[\frac{mol}{kg\ daf}]$	1.6

To get a rough estimation of how the degree of char gasification would influence the product heating value, it was assumed that the char could be represented by pure carbon and that it reacted according to the formula in Equation 1. Based on the desired char conversion, the cold gas composition from the reference case was padded with H_2 and CO according to equation 1. From this adjusted composition, a lower heating value (LHV) of the cold gas was calculated and used to find the required mass flow of biomass to the gasification chamber. The steam to biomass ratio from the reference case as well as the desired moisture content was then used to find the steam mass flow as well as the total amount of moisture to be evaporated. Given these quantities the sink term related to heating and drying was then formulated as

$$S_{G2} = -\dot{m}_{fuel,G} \cdot q_{fuel} - \dot{m}_{char,G} \cdot q_{char} - \dot{m}_{H_2O,G} \cdot q_{H_2O} \tag{6}$$

where

$$q_{fuel} = c_{p,fuel} \cdot (T_{pyro} - T_{feed}), \qquad q_{char} = c_{p,char} \cdot (T_{bed} - T_{pyro}),$$

$$q_{H_2O} = h_{H_2O}(T_{bed}) - h_{H_2O}(T_{feed}) + \Delta H_{vap,H_2O}$$

Here $h_{H_2O}(T)$ denotes the sensible heat of water at temperature T. The modeled drying process that of first heating the biomass to an assumed pyrolysis temperature, in this case 500 $°C$ was deemed adequate. In the temperature interval from pyrolysis temperature to the set bed temperature, the biomass was considered completely devolatilised and the only fraction remaining to be heated to bed temperature was taken as char. The moisture is also brought to its boiling temperature, evaporated and the resulting steam then brought to bed temperature.

In equation 6, the C_p for biomass used was obtained through a correlation from a study by Gupta *et al.* [39]. In the range studied, the correlation yielded a mean value of 1.25 $\frac{kJ}{kgK}$. The C_p for char was obtained from the same study and had a mean value of 1.53 $\frac{kJ}{kgK}$

With the heating and drying of the feedstock taken care of, the only remaining energy demanding process in the gasification chamber is the gasification of char. The sink term related to char gasification was formulated as

$$S_{G1} = \frac{m_{char}}{M_{char}} X_{char} \Delta H_r \tag{7}$$

where ΔH_r is the reaction enthalpy provided in equation 1. This treatment is an idealisation. However, it was deemed sufficient for an order of magnitude calculation.

3.2.2 Combustion chamber

The starting point for the calculation of terms in the combustion chamber was the desired load of 85 MW. Through that load and an assumed boiler efficiency, the necessary mass flow of fuel for the unaltered case could be obtained. This mass flow of fuel was then padded with a compensation term depending on the heat demand calculated for the gasification chamber.

In reality, the temperature of the bed would be controlled by regulating the air flow and running closer to, or further from, stoichiometric conditions. However, this kind of detail was de-prioritized since the main variable of interest was the temperature difference

between the chambers and not the absolute temperatures. Thus, the compensation mostly served as a way to ensure that the overall energy balance checked out.

Given the massflow of fuel to the combustion chamber the required amount of air was calculated as 60 % of that required for stoichiometric combustion given the elemental composition of the fuel. The value of 60 % is based on personal communication with representatives from the construction company. It was said that FBRs of this type generally operate under sub-stoichiometric conditions and that 60 % was a reasonable value.

Analogous to in the gasification chamber, the total amount of moisture was calculated based on the chosen moisture content of 50 % and the sink term related to heating and drying the fuel formulated as:

$$S_{C2} = -\dot{m}_{fuel,C} \cdot q_{fuel} - \dot{m}_{char,C} \cdot q_{char} - \dot{m}_{H_2O,C} \cdot q_{H_2O} \tag{8}$$

The drying process in the combustion chamber was thought to proceed in a manner analogous to that in the gasification chamber. Thus, no heat was subtracted to heat the volatile gases since they were thought to be advected out of the domain and be heated further during the gaseous combustion in the freeboard. However, the char was heated to bed temperature.

Regarding the source term for the energy due to combustion of char it was formulated as

$$S_{C1} = \left(m_{char,C} + (1 - X_{char})\, m_{char,G}\right) LHV_{char} \tag{9}$$

Most notable in equation 9 is that all the unreacted char from the gasification chamber is assumed to diffuse out and combust in the combustion chamber. This phenomenon complicates the temperature compensation scheme further since it also alters the ratios of fuel to air and fuel to moisture compared to in the unaltered bed. The heating value used for the char was that of graphite, this is a common assumption when lack of information make any detailed estimation unfeasible [22].

The last step to obtain the correct volumetric source terms was to scale the quantities described by equations 6 - 9 by the volume they were applied on. For the top sink terms S_{G2} and S_{C2} this volume was given by the crossectional area of their respective chamber and a chosen height of 0.3 m. For the remaining two terms S_{G1} and S_{C1}, the volume used was that of their respective chamber.

3.3 Mesh study

To find out what grid size would be required, and to be able to predict the time needed, a series of simulations using the same E-E framework as intended for the detailed simulation was setup but using a smaller domain. The smaller domain was chosen to be able to step down in grid size sufficiently to investigate mesh independence, but without being too time-consuming. The different grid sizes tried were 70, 50 and 30 times the particle diameter.

The model setup used was chosen to correspond to the one to be used in the detailed study, i.e a two-fluid setup with closures from the kinetic theory of granular flow as described in section 2.2.1. However, since the temperature field was assumed to depend on the flow field, without any major influence the other way around, it was deemed sufficient to only solve for momentum and mass, neglecting energy. Furthermore, without the introduction of an arbitrary source or sink term, the temperature field would have been uniform.

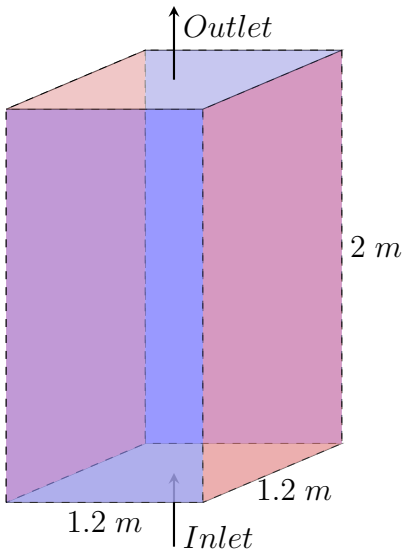

(a) The control volume used for the mesh study.The colors indicate matching periodic boundaries.

Boundary	Flow specification
Inlet :	Velocity inlet, $u = 1.5\ m/s$ $\alpha_g = 1$
Outlet :	Pressure outlet, $p = 1\ atm$ $\alpha_g = 1$
Sides :	Periodic

(b) Summary of the boundary conditions used for the mesh study.

Figures 3a and 3b show the domain used and the corresponding boundary conditions. The domain size being 1.2x1.2 m at its base was chosen since initial simulations of the entire unaltered bed showed mean bubble paths around that size. The sides of the domain were made periodic in order not to introduce any wall effects.

All numerical schemes used were of first order. The temporal discretisation used was

second order with a timestep of 10^{-4} s. This is the same setup as used for the detailed model. The maximum convective Courant number was monitored through the simulation, it was kept well below 1 at all times.

The initial state of the bed material is set to the given static bed height of 0.55 m and with a uniform volume fraction of 0.57. The value for the volume fraction is taken from the voidage at at minimum fluidisation calculated from correlations. The initial air velocity is taken as the inlet velocity compensated for the lower flow area due to the presence of particles i.e

$$u_{initial} = u_{inlet}/\alpha_g$$

Furthermore, to avoid having to spend simulation time on raising the bed from static to fluidised state several times the case was first started on the $70d_p$ mesh and ran until the bed was thoroughly fluidised. Then, at around 23 s the mesh was refined stepwise and each mesh allowed to run for a few seconds until 25 s. After that the mean field monitors were initialised and all meshes ran for an additional 7 s approximately.

Regarding material properties for the fluid and bed material they are taken at 850 $°C$ as those of air and silica, respectively. The density of the air is treated as constant.

3.4 Detailed Simulation

Based on the initial investigations as well as the mesh study it was made clear that a simulation resolving the entire domain would not be feasible given the time and resources available. To reduce the computational effort but still provide answer to the question of whether the heat transfer would be enough to sustain the gasification it was decided to only model a section of the bed. The place where the heat transfer was thought to be most critical was in the space right underneath the wall between the chambers. Thus, the domain for the detailed model was centered around a section of the dividing wall.

However, without resolving the entire bed, a treatment using source terms like those of the simplified model would be unfeasible due to the then unknown temperature field at the internal boundaries. Thus, the goal of the detailed simulation can not be a realistic temperature field of the retrofitted bed. Instead, the focus of the detailed simulation is to provide a second more applicable estimation of the effective conduction in the bed. This updated value can then be used in a reduced order model such as the simplified model developed in the pre-study.

The method used to investigate the effective conductivity is based on monitoring the heat flux through a plane just underneath the dividing wall. Given a heat flux, a known temperature difference and a fixed distance over which the heat transfer occurs, the effective conductivity can then be calculated through Fourier's law.

$$k_{eff} = \frac{q}{A} \frac{1}{\frac{\mathrm{d}T}{\mathrm{d}x}} \approx \frac{q}{A} \frac{\Delta T}{\Delta x} \tag{10}$$

A way to think about it is that the setup is in analogy to conduction through a solid slab with fixed temperatures at each side.

To ensure constant temperatures at a fixed distance from the wall, the temperature field 0.3 m into each section is frozen to a constant temperature as shown in Figure 4. The temperatures chosen correspond loosely to a desired maximum temperature difference.

The sides of the domain are made periodic in the Z-direction to reduce any possible wall effects from that side. Since the heat transfer investigated will occur in the X-direction those sides can not be made periodic as well, they are instead set to be symmetry-planes.

The model setup used here was like described previously for the mesh study that of a two-fluid model with closures from the kinetic theory of granular flow. In addition, two energy balances were solved, one for each phase. Three species balances were also included in order to allow the use of different fluidising media in the two chambers, as well as include a tracer species to track how the product gas would disperse through the domain.

Furthermore, to decrease the complexity of the setup, the energy balance of the fluidising media is entirely uncoupled from that of the bed material. The air is said to be entering the domain already at bed temperature. Furthermore, its density is assumed constant and the material properties those at 850 $^{\circ}C$.

Regarding the spatial discretisation, the numerical schemes are of first order as of yet and the grid size used is 50 particle diameters. The initial simulations as well as the mesh study had shown that a grid size smaller than that would take considerably longer time. For the temporal discretisation the time stepping is of second order and the time step $10^{-4}\,s$. The second order scheme was used since it reduced the number of inner iterations needed without any noticeable instability. The time step was chosen since it had allowed for a stable simulation in the initial simulations. Larger time steps had initially led to diverging solutions.

The boundary conditions for the simulation can be found in Table 6. Worth noting is that

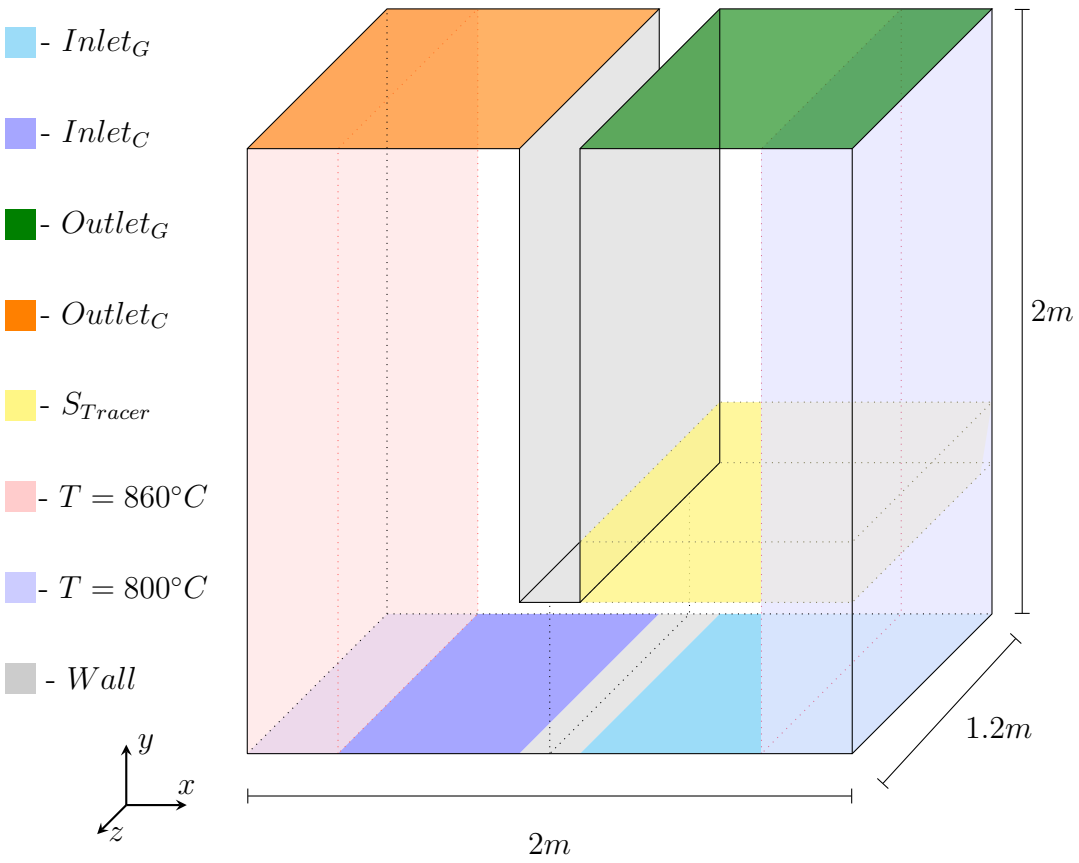

Figure 4: The domain used for the detailed study. The uncolored plane in the center is that through which the heat flux is monitored. The key S_{Tracer} stands for "source of tracer species". The thickness of the wall is 0.05 m.

the fluid velocities entering the two chambers are kept the same. These velocities does not correspond to the massflows calculated and used in the simplified model. It was however deemed at a later stage that having different levels of fluidisation in the two chambers might be difficult to handle from a process standpoint. Thus, the value of 1.2 m/s in each chamber is a compromise of the optimum calculated for each chamber, around 1.7 m/s for the combustion chamber and 0.6 m/s for the gasification chamber.

Regarding the shear stress specification on the wall, a slip condition was chosen for the solid phase. A more realistic treatment could have been possible. However, such a treatment was thought to make the simulation less stable. In addition, on industrial length-scales such as the those studied, wall effects should have less of an impact regardless of specification [37].

Table 6: The boundary conditions for the detailed model. The temperature specification refers to the temperature of an incoming flow. Thus the solid temperature specification is somewhat redundant.

Boundary	Flow specification	Temperature
$Inlet_G$	Velocity inlet: $u = 1.2\ m/s, \quad \alpha_g = 1$	$T_g = T_s = 850\ ^\circ C$
$Inlet_C$	Velocity inlet: $u = 1.2\ m/s, \quad \alpha_g = 1$	$T_g = T_s = 850\ ^\circ C$
$Outlet_C$	Pressure outlet: $p = 1\ atm, \quad \alpha_g = 1$	$T_g = T_s = 850\ ^\circ C$
$Outlet_G$	Pressure outlet: $p = 1\ atm, \quad \alpha_g = 1$	$T_g = T_s = 850\ ^\circ C$
$Sides_{X-axis}$	Symmetry plane	Symmetry plane
$Sides_{Z-axis}$	Periodic	Periodic
$Walls$	Fluid: No-slip, Solid: Slip	Adiabatic

The simulation is initialised with the bed at rest at a bed height of 0.55 m and a particle volume fraction of 0.57 in analogy with the treatment described for the mesh study. The velocity of the fluid is also initialised like in the mesh study, i.e at the inlet velocity corrected with the fluid volume fraction in the domain. As regards the species balances, the mass fractions of the steam and air in the fluid was set to unity in their respective chambers. The mass fraction of tracer was initialised as being zero.

4 Results

The following sections present selected results for each of the three studies. The results will be presented in the same order that their respective section in the method appeared.

4.1 Simplified model

Starting with the simplified model, Figure 5 shows a typical temperature profile obtained from the model. This profile was generated with source terms corresponding to 40% fuel moisture and 20 % char conversion and with an effective conduction of 36000 W/mK.

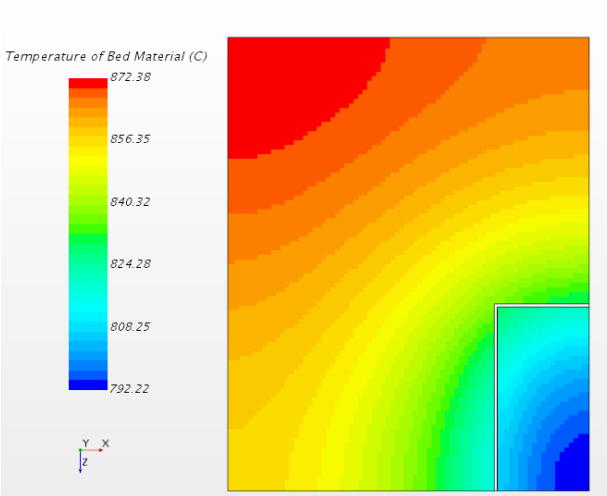

Figure 5: A typical temperature contour from the simplified model. This was generated with a fuel moisture of 40 % and the char conversion at 20 %.

The observed temperature difference of about 70 $°C$ is neither the highest nor the lowest compared to other cases.

To demonstrate the anisotropically defined conduction, Figure 6 shows the same case as in Figure 5 but from the side. Here the higher vertical conduction is clearly visible by noting that the vertical gradients are much smaller compared to the horizontal ones.

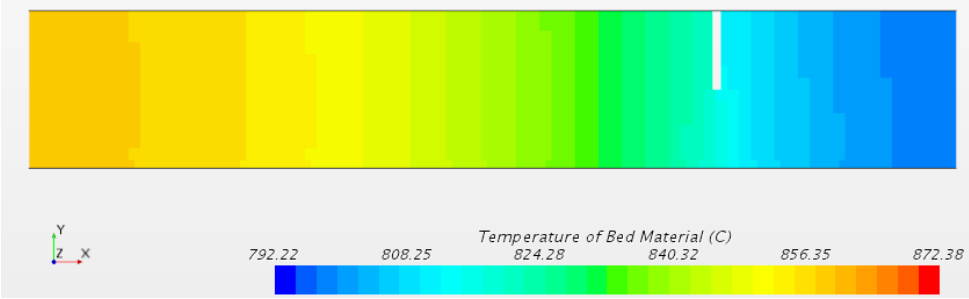

Figure 6: Side view from the same case as in Figure 5.

Additionally, the heat transfer between the gas and solid phase in this model seems

acceptable. Figure 7 shows the temperature profile for the rising air. The air can be seen entering with a low temperature but quickly getting heated to bed temperature. Only a few centimeters are needed, in accordance with the reasoning in section 2.3.

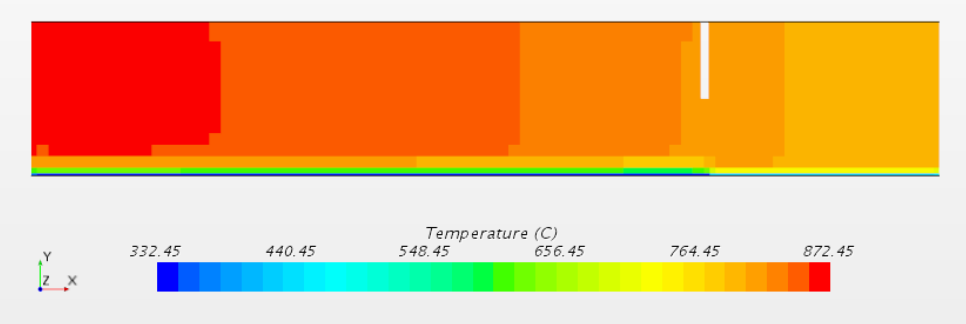

Figure 7: The temperature field of the air in the same run as shown in Figure 6.

Finally, a more practical result from the simplified model is presented. Figure 8 shows the average and maximum temperature differences observed across a series of simulations. The series was conducted using the same source terms as the above presented case but with varying values on the effective conduction. The axes for the conduction has been scaled to correspond to multiples of the previously calculated value from Zhao *et al.* It would seem that, for this case, the temperature difference reduced greatly at around 20 times the previous value. After that the temperature difference continues to decrease but at a slower rate.

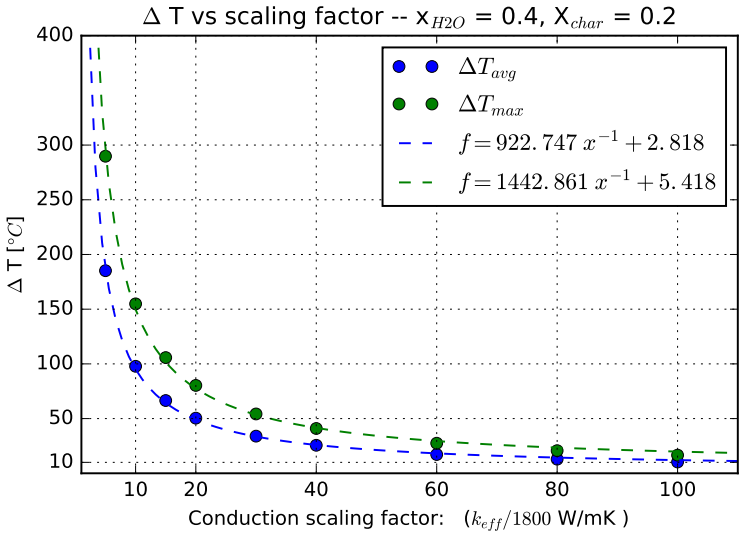

Figure 8: A series of simulations with the same conditions of 40% fuel moisture and 20 % char conversion but with varying values on the lateral conductivity

4.2 Mesh study

For the mesh study, time averaged fields for particle volume fraction for all three resolutions can be seen and compared in Figures 9a to 11b. For the topside contours the plane was located at $y = 0.45$ while for the side view at $z = 0.6$. In all three cases, there would appear to be bubble paths forming a railroad-like pattern with higher volume fractions in between. At least in the case with $30d_p$ and $50d_p$ the size of the bubbles are more or less comparable, this also applies to the distance between each denser region. For the $70d_p$ case, however, the voids formed are larger. Furthermore, in the $30d_p$ case there seems to be additional cluster structures in between the main path. Comparing with the $50d_p$ case there are indications of such structures as well, albeit more smeared. These structures are more or less non-existent in the $70d_p$ case though.

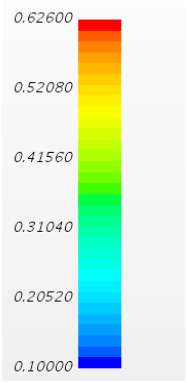

Figure 9:

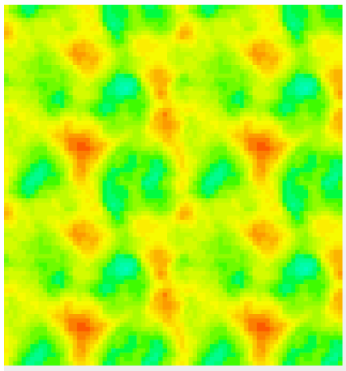

(a) Topside view of the $30d_p$-simulation

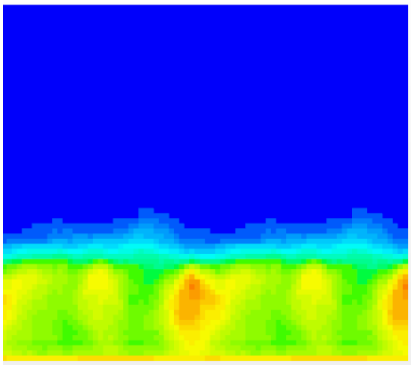

(b) Side view of the $30d_p$-simulation.

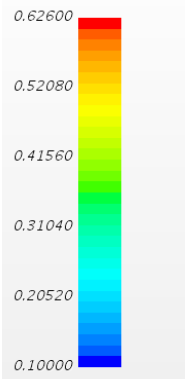

Figure 10:

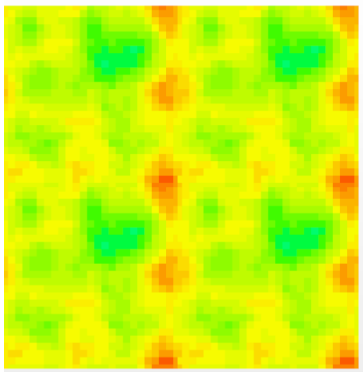

(a) Topside view of the $50d_p$-simulation

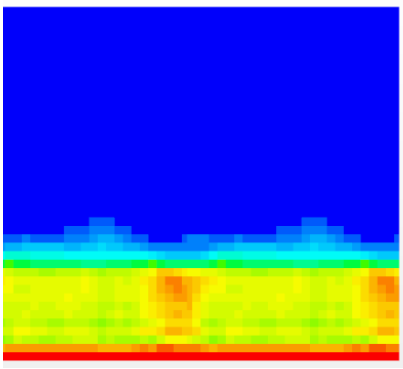

(b) Side view of the $50d_p$-simulation.

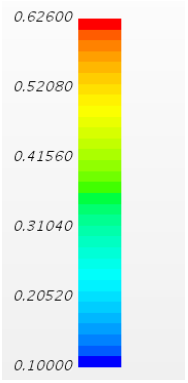

Figure 11:

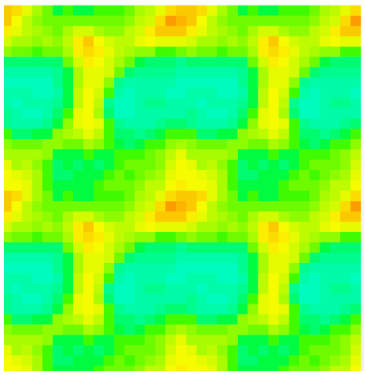

(a) Topside view of the $70d_p$-simulation

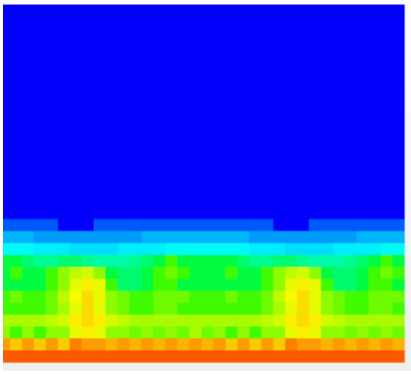

(b) Side view of the $70d_p$-simulation.

In addition to the mean fields, pressure drop and average bed height were also monitored. Figure 12a shows the pressure drop including the time before the different meshes were created. Figure 12b instead focuses on the time after mesh creation.

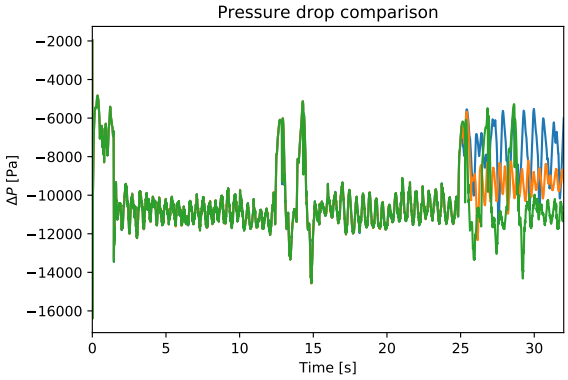

(a) The full pressure signal, starting from when the case was brought up on the $70d_p$ mesh

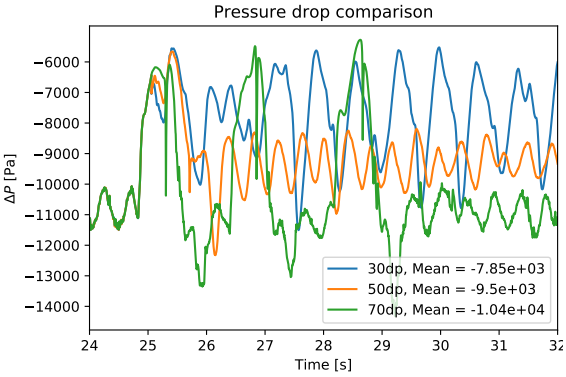

(b) The pressure signals for the individual mesh resolutions plotted together. Note the different mean levels.

Figure 12: The pressure signals for the three mesh resolutions in full and zoomed in.

It is hard to see any direct similarities between the plotted pressure drop signals. Each resolution seems to land on its own pressure level. The frequency and phase of the signals also differ. As an additional check, the average bed heights are shown in Figure 13.

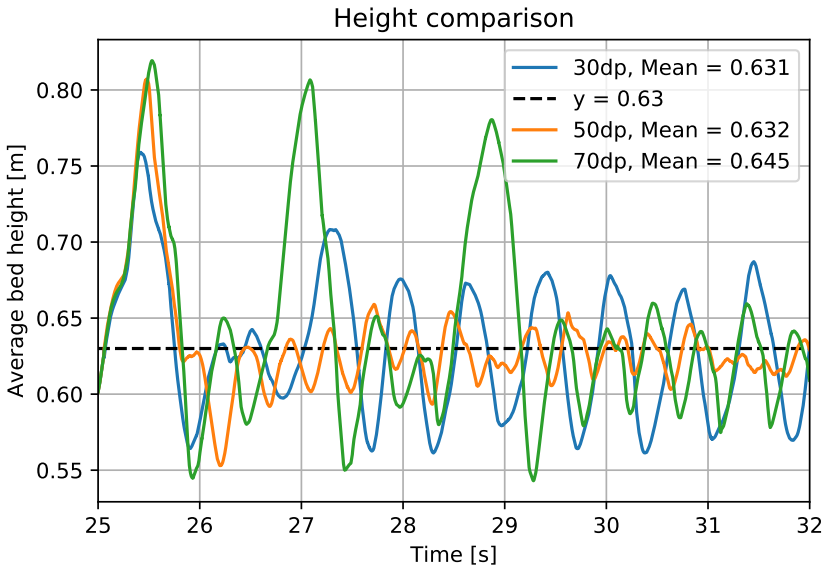

Figure 13: Average bed heights for the three mesh resolutions plotted together. The mean bed height seems to be around 0.63 m.

Here, there is a bit more similarity. It would seem that, even though the $30d_p$ signal fluctuates more, both the 50 and the 30 d_p signals land on the same mean height more or less. The $70d_p$ simulation shows some spurious peaks, however, coinciding with similar peaks in its pressure signal. Those peaks also skew the mean height.

4.3 Detailed simulation

In order to provide a feel for how the system behaves, instantaneous contours of volume fraction and temperature are presented in Figures 14a and 14b. While the volume fraction field is somewhat chaotic it is visible from the temperature field that some mixing is happening. The small region of low volume fraction below the wall stems from the fact that right under the wall there is no inlet for either air or steam. Thus, at a height sufficiently close to the floor any particles entering just drop down. Whether this behaviour is physical or not can be debated.

The most crucial information from the detailed model is of course the energy flow between the chambers. The raw signal corresponding to the instantaneous net flow of energy under the wall can be seen in Figure 15a. Obvious from the figure is that at the energy flux due to convection varies quite much and that it goes in both directions. To be able to

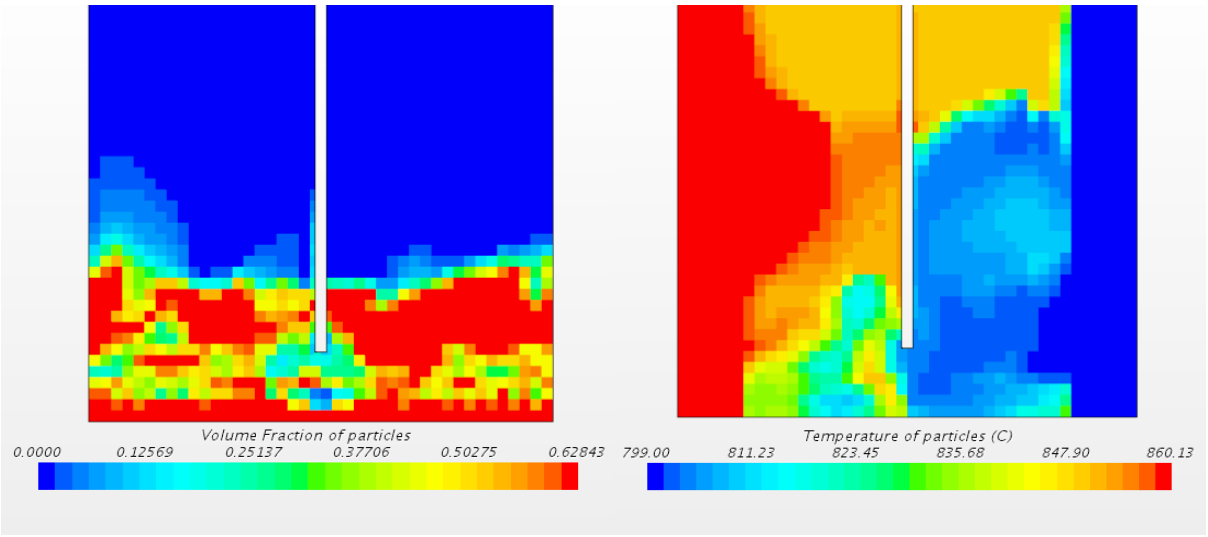

(a) Instantaneous volume fraction field for the detailed model at z=0.6 m

(b) Instantaneous temperature field for the detailed model at z=0.6 m

Figure 14: Instantaneous volume fraction and temperature field for the detailed model.

say something about the net flow for any given amount of time, the signal has to be averaged over that time period. The time averaged signal is shown with an expanding mean in Figure 15b. Together with the expanding mean is also the reversed mean. i.e the time averaged mean but calculated from the end of the data set instead of the beginning. Following the reversed mean from left to right shows what the cumulative mean would be if points of the dataset were dropped at the start. In analogy, following the unreversed mean from right to left shows the same but for points dropped at the end. It is worth noting that the unreversed mean shows greater variation at the start than the reversed mean. The greater variation could possibly indicate that the system had not reached steady-state when the averaging process started.

To further analyse the mean signal, Figure 16 shows the same plot but zoomed in closer. In addition to the mean signal, here indications of the maximum and minimum expected values are provided. The lower bound of the expected range corresponds to a k_{eff} of 36000 W/mK i.e. 20 times the previous value by Zhao *et al.* The upper bound instead corresponds to 180000 W/mK, 100 times the previous value and on par with the values reported for fuel dispersion by Sette *et al.* As can be seen from the reversed mean, the signal lands in the expected range provided that the initial second is dropped more or less. However, since the mean still shows significant fluctuations, more data is needed to be sure.

Lastly, as an added bonus the detailed study provides an indication of how the different

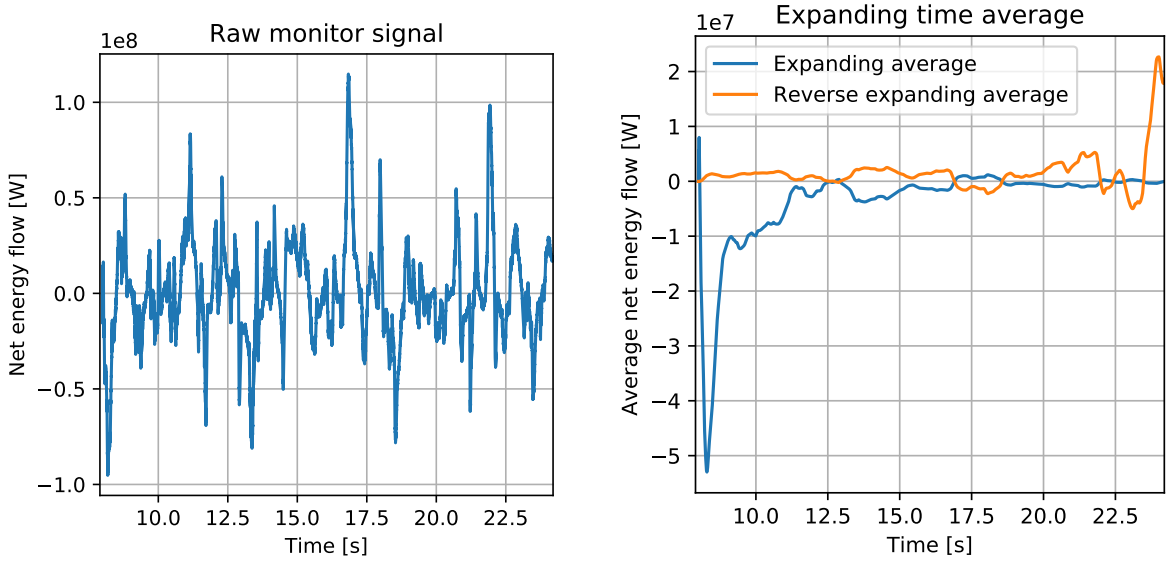

(a) The untreated signal from the energy flow monitor.

(b) The expanding mean and reversed expanding mean of the signal in (a).

Figure 15: Monitor signal for the energy flow under the wall.

gaseous species flow and disperse over time. Figure 17a shows the average mass fraction of air and Figure 17b the average mass fraction of the tracer. Note how no tracer seems to escape into the combustion chamber given this wall height. There is, however, a certain amount of air entering the gasification chamber.

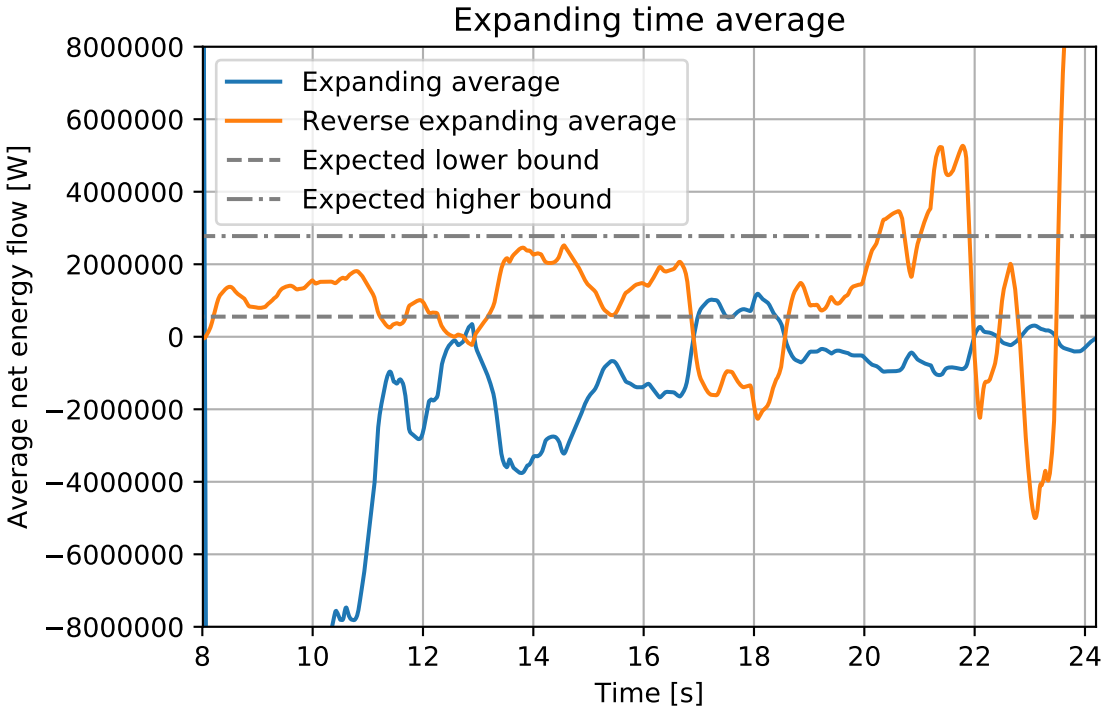

Figure 16: A zoom in on the plot provided in Figure 15b. The upper and lower bounds provided correspond to values of k_{eff} from previous studies

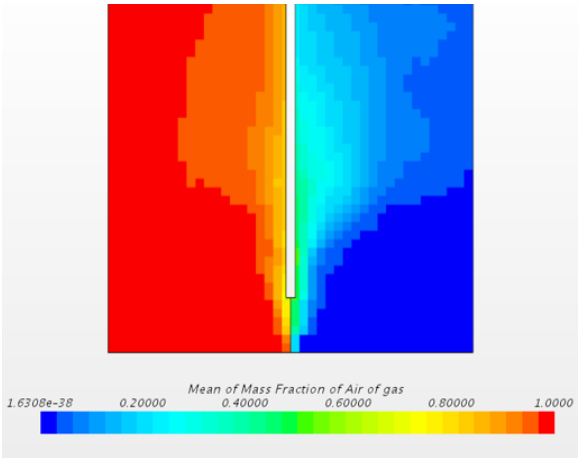

(a) Concentration of fluidisation air in the domain, shows some leakage

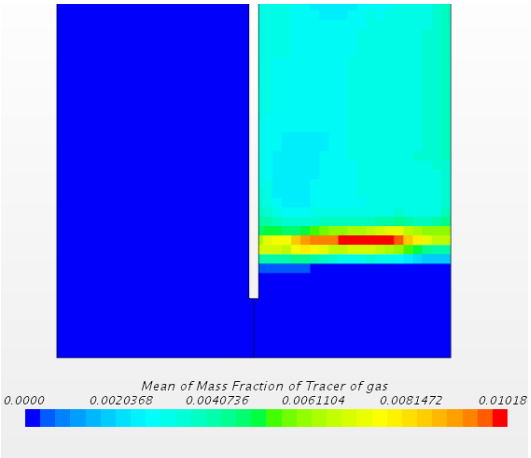

(b) Concentration of tracer species in the domain. No visible leakage.

Figure 17: Species concentrations of fluidisation gas and tracer species.

5 Discussion

Since no experimental data is available corresponding to the studied case and, not surprisingly due to the novel nature of the concept, no similar case can be found documented; many of the parameters and properties are based on estimations, assumptions, or straight up guesswork. While it would be surprising to find the estimations completely out of the window, it should be more or less expected that at least some of them will be significantly off. Some further work will have to go into crosschecking the assumptions as soon as new information becomes available. Furthermore, due to the time demand inherent in these simulations, the data available is often limited and additional uncertainties are introduced as a consequence. The following sections address many of the concerns present in the models used and provide an outlook for further work.

5.1 Ethical, environmental and societal aspects

Regarding the ethical and societal aspects of this work, no real concerns have been identified, neither in the work itself nor in the implementation of the reactor concept. The study is based on computer models alone and thus have had minimal impact on any human or animal well-being. The implementation of the reactor concept should if done correctly not affect the overall operation of the plant it is installed in to any big degree.

Regarding the ecological aspects there might be a slight impact on certain forest ecosystems if forestry litter is collected for use in gasification specifically. However, to say that the collection of forestry litter is governed by the need for gasification feedstocks is a stretch. If the technology gains widespread use it might very well lead to decreased greenhouse gas emmissions as fossil gas can be replaced. Widespread adoption could also in the long run lead to greater need for woody biomass, which could put greater strain on our forests. With correct regulations however a balance that makes good use of our forests while preserving species diversity should be possible.

5.2 Simplified model

For the simplified model, the greatest point of concern is likely the calculation of the source terms used to drive the heat transfer. Since most data is based on a single case, not necessarily corresponding to the current setup in terms of fuel type or overall operating conditions, there are bound to be discrepancies there. However, as the project moves along

and more data from the various other supprojects comes in, most of those assumptions can likely be verified or at least strenghtened. Given more confident footing regarding the source terms, the overall results from the model should be more reliable.

Besides the actual value of the source terms, the implementation of them of course matters as well. In reality, the fuel would not be perfectly mixed over the domain, thus the even placement of the source terms might be more or less suitable. A changed placement could probably affect the overall temperature field and introduce new gradients at certain points possibly changing the temperature in the gasification chamber for better or for worse. However, since the source terms are based on overall balances of the system, the general picture should not change that much. Furthermore, the effects of uneven feeding should be somewhat regulated since the amount of air entering is the limiting factor and can be controlled externally.

From a modelling point of view rather than a physical point of view, it should be noted that no investigation into the eventual mesh dependency of the model has been done. If a finer mesh would result in tighter gradients than the maximum temperature difference would likely go down. Thus, probably the current mesh at least does not overestimate the heat transfer.

A way in which the model could be improved is likely by introducing mass and momentum terms due to the addition of fuel and non-equimolar gasification reaction, respectively. In the initial stage of the project, the amount of fuel accumulated in the bed was thought to be so little as to be insignificant; however, at later discussions values around 20 % of the bed mass have been mentioned. Speculatively, the missing char mass probably does not influence the result that much but it is easy to verify. Also, the air should have some added momentum due to the non-equimolar char conversion reaction, eq (1). However, since the char conversion is projected to be low and the convection only has a minor effect on the bed temperature, this effect is probably also has lower impact.

Another improvement would be to introduce a species balance to allow having steam as a fluidising agent. Since steam has about double the C_p as air it would likely introduce a greater heat load. The greater heat load could probably influence the overall temperature field to some extent. Lastly, another likely significant improvement is to include the fact that the bed has a sand return system where sand goes out in the bottom of the boiler, is cooled and the reinjected at the top. Due to its high thermal mass, a flow of cool bed material has the potential to skew the temperature profile somewhat.

5.3 Mesh study

Regarding the mesh study it is obvious at least from the pressure drops in Figure 12b, that there is a mesh-dependency in the current solution using $50d_p$-gridsize. From looking at the mean fields there is an indication of neglected clustering effects in the $50d_p$ simulation. However, comparing to the $70d_p$ case, it is obvious that the 50 and 30 dp cases are closer. Thus, it would seem like the simulation is positioned on the way to mesh independence but not quite there.

The most important question in relation to the grid size is of course how much this discrepancy is likely to affect the particle dispersion and thereby heat conduction. If the simulation is still mesh dependent, a reasonable assumption to make is that the addition of more cells would yield more and finer flow structures, if not only because the larger amount of cells provide more ways for particles and bubbles to arrange. It would seem reasonable that more and finer structures would lead to greater variation in the flow field. This greater variation with increasing mesh density is also visible to some degree in the greater fluctuations around the mean seen in the $30d_p$ pressure and bed height signals. More ways to rearrange should reasonably lead to higher gas and particle dispersion values rather than lower. Thus, the discrepancy should probably lead to an underestimated or conservative estimation of the k_{eff} which is what is desired from a design calculation perspective. However, this line of reasoning needs to be verified by similar grid-independence studies from literature before it is to be regarded as anything other than speculation.

5.4 Detailed model

As visible from the still fluctuating average in Figure 16, the detailed simulation has to run more before any conclusive results regarding heat transfer can be obtained. Furthermore, there is the question of whether to drop some initial data to be sure that no initial transient related to the initialisation is captured. If that is to be done, however, either the simulation needs to be run for a sufficiently long time as to make a few seconds insignificant or some method of discerning the transient has to be employed. It would seem that further analysis of the data is in order.

Furthermore, the detailed simulation is a rather idealized case, the frozen temperature fields as well as the uncoupled fluid energy balance clearly put the case at more of a laboratory setting than an entirely natural one. When it comes to the uncoupled fluid energy, the reasoning is easy. The implementation would simply have been more trouble than what it would be worth. If the detailed model had included heating of the fluidising

media, additional source terms would have been needed to account for that heat. Without modelling the entire bed, these source terms would have to be of a mathematical rather than physical origin. In addition, the results from the simplified model shows that while a small vertical temperature gradient exists on the fluid side, it is much less pronounced on the bed side due to the higher thermal mass of the bed material. Furthermore, an added heat transfer mechanism by transfer with the fluid would, regardless of whether it is significant or not, likely serve to enhance the heat transfer in this case. Thus, by neglecting it, the model is providing an underestimated value which, again, is fine from a design calculation perspective.

The fixed temperatures are a bit harder to motivate entirely. By freezing the temperatures at a specific distance from each other, the model essentially decides both the temperature gradient and the distance for conduction. If this had been a true heat transfer controlled problem, the temperature gradient would be the driving force; so, by fixing that the conduction would be influenced as well. However, in this case it is not the temperature gradient that is the dominant driving force but rather the bed movement. The bed movement will be the same more or less regardless of the temperature field. Since the temperature difference and distance dictate the energy flow, and these values are used together to obtain the value for k_{eff}, the temperature difference should be arbitrary. However, if a smaller temperature difference had been used, the overall fluctuations around the mean seen in the energy flow signal would likely not be as large. Reduced fluctuations could be a good thing if it reduces the time needed to obtain a stable average.

Another point worthy of discussion is the deadzone under the wall, i.e the region with no inlet underneath. It clearly has an effect on the flow. A more reasonable approach would probably be to extend the gasification inlet outward so it touches the combustion inlet. That would be closer to the planned construction as well. However, it should be noted that in reality the fluidising media would not be injected in a uniform distribution like the one simulated but rather in through an array of nozzles linked hydrodynamically through a common plenum. The pressure inside the plenum and the spacing of the nozzles provide further complexity. Unfortunately, the nozzles are too small to be resolved correctly by the coarse grid used and the additional complexity might very well introduce instability. In a future study, it would, however, be beneficial to discern the overall difference between the porous plate arrangement used and that of one with nozzles and plenum.

Another point that definitely deserves further study is the impact the distance between the wall and the floor has on the flow. It is reasonable to assume that a larger window would be less restrictive to the flow and therefore hinder heat transfer less. On a related note, the thickness of the wall could also be important. The one used in the study is most likely too thin compared to the one that will be used, if the thickness has a major impact on the flow, it would be beneficial to know that.

Lastly, from a modelling point of view, it should be noted that no investigation as to the effect of the submodels used to close the TFM has been done. While several studies show that some of the submodels are rather interchangeable for some things like bed expansion and pressure drop [10], the actual flow structure in the simulations could very well be different. As an example, in an article by Farzaneh *et al.* [40], three different models for frictional stress, $\tau_{\mathbf{f}}\mathbf{r}$, are compared. In the article, it is shown that depending on what model is used the dispersion of fuel particles differs. In addition, in some cases there were differences in how many vortexes there were present in the bed. Thus, the model choice in the study presents a further degree of uncertainty. The choice of models as it stands now is largely dictated by the available setup in the software. Thus, a more thorough investigation into recommended models might lead to a change of software.

5.5 Concluding discussion

To conclude, the current outlook, at least what can be gleaned from the simplified model, suggests that the retrofit might indeed be viable from a heat transfer point of view. Depending on the outcome of the detailed study this can of course change, but not only for the worse.

If I was to answer the question of whether the temperature in the gasification chamber will be high enough to support gasification the answer would be yes. However, to what degree and with what resulting gas composition and need for refining remains to be seen.

Regarding the question of gas leakage between the chambers, the current simulations indicate that any product gas leaking will be minor. Depending on how the air and steam inlet is positioned there will be some mixing there. However, by shifting either inlet to one side it should be possible to control what fluid leaks where.

Still many uncertain points remain to be assessed in several parts of the project, but as new data becomes available regarding the other subprojects, the used models will be updated. Further work and experimental validation is needed to completely verify the effective conduction.

References

[1] J. Werther, E.-U. Hartge and S. Heinrich, 'Fluidized-Bed Reactors - Status and Some Development Perspectives', *Chemie Ingenieur Technik*, vol. 86, no. 12, pp. 2022–2038, Dec. 2014, ISSN: 0009286X. DOI: 10.1002/cite.201400117. [Online]. Available: http://doi.wiley.com/10.1002/cite.201400117.

[2] W. Letzsch, 'Fluid catalytic cracking (FCC)', in *Handbook of Petroleum Processing*, D. S. J. S. Jones and P. R. Pujadó, Eds., Dordrecht: Springer Netherlands, 2006, pp. 239–286, ISBN: 978-1-4020-2820-5. DOI: 10.1007/1-4020-2820-2{_}6. [Online]. Available: https://doi.org/10.1007/1-4020-2820-2_6.

[3] J. Hammerschmidt, J. Güntner and B. Kerstiens, 'Roasting of gold ore in the circulating fluidized-bed technology', *Developments in Mineral Processing*, vol. 15, pp. 433–453, Jan. 2005, ISSN: 0167-4528. DOI: 10.1016/S0167-4528(05)15018-2. [Online]. Available: https://www.sciencedirect.com/science/article/pii/S0167452805150182.

[4] J. Werther, Werther and Joachim, 'Fluidized-Bed Reactors', in *Ullmann's Encyclopedia of Industrial Chemistry*, Weinheim, Germany: Wiley-VCH Verlag GmbH & Co. KGaA, Apr. 2007, ISBN: 9783527306732. DOI: 10.1002/14356007.b04{_}239.pub2. [Online]. Available: http://doi.wiley.com/10.1002/14356007.b04_239.pub2.

[5] E. Anthony, 'Fluidized bed combustion of alternative solid fuels; status, successes and problems of the technology', *Progress in Energy and Combustion Science*, vol. 21, no. 3, pp. 239–268, Jan. 1995, ISSN: 0360-1285. DOI: 10.1016/0360-1285(95)00005-3. [Online]. Available: https://www.sciencedirect.com/science/article/pii/0360128595000053?via%5C%3Dihub.

[6] K. Göransson, U. Söderlind, J. He and W. Zhang, 'Review of syngas production via biomass DFBGs', *Renewable and Sustainable Energy Reviews*, vol. 15, no. 1, pp. 482–492, Jan. 2011, ISSN: 1364-0321. DOI: 10.1016/J.RSER.2010.09.032. [Online]. Available: https://www.sciencedirect.com/science/article/pii/S1364032110003199.

[7] T. Mattisson, A. Lyngfelt and H. Leion, 'Chemical-looping with oxygen uncoupling for combustion of solid fuels', *International Journal of Greenhouse Gas Control*, vol. 3, no. 1, pp. 11–19, Jan. 2009, ISSN: 1750-5836. DOI: 10.1016/J.IJGGC.2008.06.002. [Online]. Available: https://www.sciencedirect.com/science/article/pii/S1750583608000510?via%5C%3Dihub.

[8] K. Zhao, H. Thunman, D. Pallarès and H. Ström, 'Control of the solids retention time by multi-staging a fluidized bed reactor', *Fuel Processing Technology*, vol. 167, pp. 171–182, Dec. 2017, ISSN: 0378-3820. DOI: 10.1016/J.FUPROC.2017.06.027. [Online]. Available: https://www.sciencedirect.com/science/article/pii/S0378382016311900.

[9] L. Glicksman, M. Hyre and P. Farrell, 'Dynamic similarity in fluidization', *International Journal of Multiphase Flow*, vol. 20, pp. 331–386, Aug. 1994, ISSN: 0301-9322. DOI: 10.1016/0301-9322(94)90077-9. [Online]. Available: https://www.sciencedirect.com/science/article/pii/0301932294900779?via%5C%3Dihub.

[10] B. G. M. van Wachem, J. C. Schouten, C. M. van den Bleek, R. Krishna and J. L. Sinclair, 'Comparative analysis of CFD models of dense gas–solid systems', *AIChE Journal*, vol. 47, no. 5, pp. 1035–1051, May 2001, ISSN: 00011541. DOI: 10.1002/aic.690470510. [Online]. Available: http://doi.wiley.com/10.1002/aic.690470510.

[11] P. Basu, *Combustion and Gasification in Fluidized Beds*. CRC Press, Feb. 2006, ISBN: 978-0-8493-3396-5. DOI: 10.1201/9781420005158. [Online]. Available: https://www.taylorfrancis.com/books/9781420005158.

[12] S. Oka and E. Anthony, *Fluidized bed combustion*. M. Dekker, 2004, ISBN: 0-8247-4699-6.

[13] M. Syamlal, W. Rogers and T. J. O'brien, '(DE94000087) MFIX Documentation Theory Guide Technical Note', Tech. Rep., 1993. [Online]. Available: https://mfix.netl.doe.gov/download/mfix/mfix_legacy_manual/Theory.pdf.

[14] A. J. Ragauskas, C. K. Williams, B. H. Davison, G. Britovsek, J. Cairney, C. A. Eckert, W. J. Frederick, J. P. Hallett, D. J. Leak, C. L. Liotta, J. R. Mielenz, R. Murphy, R. Templer and T. Tschaplinski, 'The path forward for biofuels and biomaterials.', *Science (New York, N.Y.)*, vol. 311, no. 5760, pp. 484–9, Jan. 2006, ISSN: 1095-9203. DOI: 10.1126/science.1114736. [Online]. Available: http://www.ncbi.nlm.nih.gov/pubmed/16439654.

[15] Z. A. B. Z. Alauddin, P. Lahijani, M. Mohammadi and A. R. Mohamed, 'Gasification of lignocellulosic biomass in fluidized beds for renewable energy development: A review', *Renewable and Sustainable Energy Reviews*, vol. 14, no. 9, pp. 2852–2862, Dec. 2010, ISSN: 1364-0321. DOI: 10.1016/J.RSER.2010.07.026. [Online]. Available: https://www.sciencedirect.com/science/article/pii/S1364032110002066#bib0210.

[16] A. Larsson, M. Seemann, D. Neves and H. Thunman, 'Evaluation of Performance of Industrial-Scale Dual Fluidized Bed Gasifiers Using the Chalmers 2–4-MW _{th} Gasifier', *Energy & Fuels*, vol. 27, no. 11, pp. 6665–6680, Nov. 2013, ISSN: 0887-0624. DOI: 10.1021/ef400981j. [Online]. Available: http://pubs.acs.org/doi/10.1021/ef400981j.

[17] G. Schuster, G. Löffler, K. Weigl and H. Hofbauer, 'Biomass steam gasification – an extensive parametric modeling study', *Bioresource Technology*, vol. 77, no. 1, pp. 71–79, Mar. 2001, ISSN: 0960-8524. DOI: 10.1016/S0960-8524(00)00115-2. [Online]. Available: https://www.sciencedirect.com/science/article/pii/S0960852400001152.

[18] D. Burgess, 'Thermochemical Data', in *NIST Chemistry WebBook, NIST Standard Reference Database Number 69*, P. Linstrom and W. Mallard, Eds., Gaithersburg MD 20899: National Institute of Standards and Technology. DOI: 10.18434/T4D303. [Online]. Available: https://doi.org/10.18434/T4D303.

[19] M. Puig-Arnavat, J. C. Bruno and A. Coronas, 'Review and analysis of biomass gasification models', *Renewable and Sustainable Energy Reviews*, vol. 14, no. 9, pp. 2841–2851, Dec. 2010, ISSN: 1364-0321. DOI: 10.1016/J.RSER.2010.07.030. [Online]. Available: https://www.sciencedirect.com/science/article/pii/S1364032110002108#bib0295.

[20] M. Ã–hman, A. Nordin, B.-J. Skrifvars, R. Backman and M. Hupa, 'Bed agglomeration characteristics during fluidized bed combustion of biomass fuels', *Energy & Fuels*, vol. 14, no. 1, pp. 169–178, 2000. DOI: 10.1021/ef990107b. eprint: https://doi.org/10.1021/ef990107b. [Online]. Available: https://doi.org/10.1021/ef990107b.

[21] D. Neves, H. Thunman, A. Matos, L. Tarelho and A. Gómez-Barea, 'Characterization and prediction of biomass pyrolysis products', *Progress in Energy and Combustion Science*, vol. 37, no. 5, pp. 611–630, Sep. 2011, ISSN: 0360-1285. DOI: 10.1016/J.PECS.2011.01.001. [Online]. Available: https://www.sciencedirect.com/science/article/pii/S0360128511000025?via%5C%3Dihub.

[22] Henrik Thunman, Fredrik Niklasson, Filip Johnsson and Bo Leckner, 'Composition of Volatile Gases and Thermochemical Properties of Wood for Modeling of Fixed or Fluidized Beds', 2001. DOI: 10.1021/EF010097Q. [Online]. Available: https://pubs-acs-org.proxy.lib.chalmers.se/doi/abs/10.1021/ef010097q.

[23] A. Roberts, 'The heat of reaction during the pyrolysis of wood', *Combustion and Flame*, vol. 17, no. 1, pp. 79–86, Aug. 1971, ISSN: 0010-2180. DOI: 10.1016/S0010-2180(71)80141-4. [Online]. Available: https://www.sciencedirect.com/science/article/pii/S0010218071801414.

[24] E. Michaelides, C. T. Crowe, J. D. Schwarzkopf, C. T. Crowe and J. D. Schwarzkopf, *Multiphase Flow Handbook*, E. E. Michaelides, C. T. Crowe and J. D. Schwarzkopf, Eds., ser. The CRC Press Series in Mechanical and Aerospace Engineering. Taylor & Francis Group, 6000 Broken Sound Parkway NW, Suite 300, Boca Raton, FL 33487-2742: CRC Press, Sep. 2016, ISBN: 978-1-4987-0100-6. DOI: 10.1201/9781315371924. [Online]. Available: https://www.taylorfrancis.com/books/9781498701013.

[25] C. K. K. Lun, S. B. Savage, D. J. Jeffrey and N. Chepurniy, 'Kinetic theories for granular flow: inelastic particles in Couette flow and slightly inelastic particles in a general flowfield', *Journal of Fluid Mechanics*, vol. 140, no. -1, p. 223, Mar. 1984, ISSN: 0022-1120. DOI: 10.1017/S0022112084000586. [Online]. Available: http://www.journals.cambridge.org/abstract_S0022112084000586.

[26] S. Chapman and T. G. Cowling, *Mathematical Theory of Non-Uniform Gases.* Ser. Cambridge Mathematical Library. Cambridge : Cambridge U P, 1970., 1970, ISBN: 0-521-40844-x. [Online]. Available: http://proxy.lib.chalmers.se/login?url=http://search.ebscohost.com/login.aspx?direct=true&db=cat06296a&AN=clc.b1176589&lang=sv&site=eds-live&scope=site.

[27] S. B. Savage and D. J. Jeffrey, 'The stress tensor in a granular flow at high shear rates', *Journal of Fluid Mechanics*, vol. 110, pp. 255–272, 1981. DOI: 10.1017/S0022112081000736.

[28] J. Garside and M. R. Al-Dibouni, 'Velocity-Voidage Relationships for Fluidization and Sedimentation in Solid-Liquid Systems', *Industrial & Engineering Chemistry Process Design and Development*, vol. 16, no. 2, pp. 206–214, Apr. 1977, ISSN: 0196-4305. DOI: 10.1021/i260062a008. [Online]. Available: http://pubs.acs.org/doi/abs/10.1021/i260062a008.

[29] J. M. DallaValle and A. Klemin, *Micromeritics: the technology of fine particles.* New York: Pitman Pub. Corp., 1943, xiv, 428 p. Bibliography: p. 377-415. [Online]. Available: //catalog.hathitrust.org/Record/001512807.

[30] S. Ogawa, A. Umemura and N. Oshima, 'On the equations of fully fluidized granular materials', *Zeitschrift für angewandte Mathematik und Physik ZAMP*, vol. 31, no. 4, pp. 483–493, Jul. 1980, ISSN: 0044-2275. DOI: 10.1007/BF01590859. [Online]. Available: http://link.springer.com/10.1007/BF01590859.

[31] D. Gidaspow, R. Bezburuah and J. Ding, *Hydrodynamics of circulating fluidized beds: Kinetic theory approach*, Jan. 1991. [Online]. Available: https://www.osti.gov/biblio/5896246.

[32] D. G. Schaeffer, 'Instability in the evolution equations describing incompressible granular flow', *Journal of Differential Equations*, vol. 66, no. 1, pp. 19–50, Jan. 1987, ISSN: 0022-0396. DOI: 10.1016/0022-0396(87)90038-6. [Online]. Available: https://www.sciencedirect.com/science/article/pii/0022039687900386.

[33] S. Cloete, S. T. Johansen and S. Amini, 'Grid independence behaviour of fluidized bed reactor simulations using the Two Fluid Model: Effect of particle size', *Powder Technology*, vol. 269, pp. 153–165, Jan. 2015, ISSN: 0032-5910. DOI: 10.1016/J.POWTEC.2014.08.055. [Online]. Available: https://www.sciencedirect.com/science/article/pii/S0032591014007657?via%5C%3Dihub.

[34] Y. Igci, A. T. Andrews, S. Sundaresan, S. Pannala and T. O'Brien, 'Filtered two-fluid models for fluidized gas-particle suspensions', *AIChE Journal*, vol. 54, no. 6, pp. 1431–1448, Jun. 2008, ISSN: 00011541. DOI: 10.1002/aic.11481. [Online]. Available: http://doi.wiley.com/10.1002/aic.11481.

[35] M. H. Uddin and C. J. Coronella, 'Effects of grid size on predictions of bed expansion in bubbling fluidized beds of Geldart B particles: A generalized rule for a grid-independent solution of TFM simulations', *Particuology*, vol. 34, pp. 61–69, Oct. 2017, ISSN: 1674-2001. DOI: 10.1016/J.PARTIC.2016.12.002. [Online]. Available: https://www.sciencedirect.com/science/article/pii/S1674200117300524?via%5C%3Dihub#bbib0115.

[36] E. Sette, D. Pallarès and F. Johnsson, 'Experimental quantification of lateral mixing of fuels in fluid-dynamically down-scaled bubbling fluidized beds', *Applied Energy*, vol. 136, pp. 671–681, Dec. 2014, ISSN: 0306-2619. DOI: 10.1016/J.APENERGY.2014.09.075. [Online]. Available: https://www.sciencedirect.com/science/article/pii/S030626191401023X?via%5C%3Dihub.

[37] F. Niklasson, H. Thunman, F. Johnsson and B. Leckner, 'Estimation of solids mixing in a fluidized-bed combustor', 2002. DOI: 10.1021/IE020173S. [Online]. Available: https://pubs.acs.org/doi/abs/10.1021/ie020173s.

[38] E. Sette, D. Pallarès and F. Johnsson, 'Experimental evaluation of lateral mixing of bulk solids in a fluid-dynamically down-scaled bubbling fluidized bed', *Powder Technology*, vol. 263, pp. 74–80, Sep. 2014, ISSN: 0032-5910. DOI: 10.1016/J.POWTEC.2014.04.091. [Online]. Available: https://www.sciencedirect.com/science/article/pii/S0032591014004318?via%5C%3Dihub.

[39] M. Gupta, J. Yang and C. Roy, 'Specific heat and thermal conductivity of softwood bark and softwood char particles', *Fuel*, vol. 82, no. 8, pp. 919–927, May 2003, ISSN: 0016-2361. DOI: 10.1016/S0016-2361(02)00398-8. [Online]. Available: https://www.sciencedirect.com/science/article/pii/S0016236102003988?via%5C%3Dihub.

[40] M. Farzaneh, A.-E. Almstedt, F. Johnsson, D. Pallarès and S. Sasic, 'The crucial role of frictional stress models for simulation of bubbling fluidized beds', *Powder Technology*, vol. 270, pp. 68–82, Jan. 2015, ISSN: 0032-5910. DOI: 10.1016/J.POWTEC.2014.09.050. [Online]. Available: https://www.sciencedirect.com/science/article/pii/S003259101400850X?via%5C%3Dihub.